ATISAI-S-No. 666518

CARDE TECHNICAL LETTER 1084/57

Copy No. 30.

Classification unchanged / changed to UNCLASS/unlimited
By authority of DREV DRP 461
Date 31/1/87 #1101/99
Signature D. Russell Baubrey
Unit / Rank / Appointment CRAD/DSIS

UNCLASSIFIED

#303817
58-06830

This information is furnished ... the Department of Defense of the United States ... specified and that it by the Department ...

CF-105 AIRCRAFT INTERCEPTOR PLACEMENT PROBLEM

3-DIMENSIONAL REAC SIMULATION

by

D. Tait

LIBRARY
JUN 23 1958
DEFENCE RESEARCH MEDICAL LABORATORIES

EXCLUDED FROM AUTOMATIC REGRADING
DOD DIR 5200.10 DOES NOT APPLY

DEFENCE RESEARCH BOARD

CANADIAN ARMAMENT RESEARCH AND DEVELOPMENT ESTABLISHMENT

Enclosure (8) to CNO Serial 004955 P92

Valcartier, Quebec

February, 1958

66 01 1193
6517005-01

EE91524

NOTE

Technical Letters are informal notes on work currently in progress and are therefore highly tentative in content. They do not necessarily reflect the opinions of the Establishment. Constructive criticisms are invited.

Carde Technical Letter 1084/57

UNCLASSIFIED

P.C.C. D46-97-36-21

Classification cancelled / changed to UNCLASS/UNLIMITED
By authority of DREV DRP 461
Date 21/1/87
Signature
Unit / Rank / Appointment CRAD/DSIS

CF-105 AIRCRAFT INTERCEPTOR PLACEMENT PROBLEM

3-DIMENSIONAL REAC SIMULATION

by

D. Tait

Analysis Group

"G" Wing

CANADIAN ARMAMENT RESEARCH AND DEVELOPMENT ESTABLISHMENT

January, 1958

65117005-01

TABLE OF CONTENTS

1.0	INTRODUCTION page	1
2.0	SUMMARY	1
	2.1 The Geometry of the Situation in Space	1
	2.2 The Fire Control Computer	1
	2.3 The Aerodynamic Performance of the CF-105 Interceptor	1
	2.4 The Capabilities of the Interceptor Weapons —	1
	2.5 The Performance of a Simplified Target	1
3.0	LIST OF SYMBOLS	2
4.0	ANALYSIS OF THE INTERCEPTION PROBLEM	4
	4.1 Geometry	4
	4.2 Heading Error	5
	4.3 Aircraft Performance	6
	4.4 Launch Zone	7
	4.5 Radar Antenna Deflections	8
5.0	AN ASSESSMENT OF THE ACCURACY OF THE REAC STUDY	8
	5.1 Geometry	8
	5.2 Aircraft Performance	11
	5.3 Launch Zone	12
	5.4 Ideal Heading Calculation	12
	5.5 Calculating of the Components of Heading Error	12
	5.6 Heading Error Calculation	13
	5.7 Effect of Neglecting Target Evasion after Launch	14
	5.8 Look Angle Barriers and the Axis Transformation	15
	5.9 Errors in the Axis Transformation System	16
	5.10 Dynamic Lags in the System	17
	5.10.1 Spurious Dynamic Lags	17
	5.10.2 Real Lags	
6.0	SNAP-UP ATTACKS	18
	6.1 Circuit Changes to Include Snap-up	
7.0	CONCLUSIONS	20
8.0	OUTPUT EQUIPMENT	20
9.0	ACKNOWLEDGEMENTS	21
10.0	REFERENCES	21
	Figures from 1 to 39	23 to 61

1.0 INTRODUCTION

CARDE has been carrying out a program to assess the effectiveness of a supersonic interceptor system. The system is based on the AVRO CF-105 aircraft armed with Sparrow II or Sparrow III air-to-air missiles. An analog computer model has been made to study the AI radar controlled phase of the interceptions.

The results of the three dimensional placement studies using this model are given in the CARDE progress reports on the CF-105 Weapon System Assessment. So that the order of accuracy of these results may be appreciated, the REAC model is discussed in some detail in this report.

In order to fit the problem to a 120 amplifier analog computer it has been necessary to simplify the model. This report is intended to describe the circuits which were used and to give some idea of the effects of the simplifications on the accuracy of the results.

Fig. 1 shows a block diagram of the computer layout.

2.0 SUMMARY

The simulation covers the following subjects.

2.1 The geometry of the situation in space with:

Target altitudes of 50,000 feet to 80,000 feet,
Fighter altitudes from 40,000 feet to 73,000 feet
For ranges up to 400K feet at all aspects for all course differences.

2.2 The Fire control computer which is designed for the following attack modes, lead collision, lead pursuit and snap-up.

The model is easily adapted to cover other attack modes involving the system parameters.

2.3 The aerodynamic performance of the CF-105 interceptor based on the latest available AVRO data. An overriding maximum speed of M 2.0 is assumed. The aircraft flies with maximum thrust until this speed is reached.

2.4 The capabilities of the interceptor weapons are used to define a launch zone and to judge the final success of the AI controlled phase.

2.5 The performance of a simplified target which can fly with constant speed and constant turn rate at altitudes from 50,000 feet to 80,000 feet at speeds up to M 4.0.

Calculations involving the computer approximations have been carried out. The effects on the placement zone boundaries are quite small. Figure 26 gives a typical placement zone with the effects of the errors shown on it. These errors are converted into placement probability in Fig. 27.

3.0 LIST OF SYMBOLS

A	horizontal component of aspect angle of fighter measured from the tail of its target.
B	inclination of the line of sight to the horizontal
D	fighter drag
D_o	drag at zero lift
$\underline{F}$	vector distance travelled by a missile fired from the fighter relative to the fighter
F	distance between missile and fighter t_f seconds after launch
g	acceleration due to gravity
K'	navigation turn-rate to error ratio (see equations 25 & 26)
K	maximum value of K' (see equations 21 & 22)
L	lift
L_m	maximum allowable lift
L_a	interceptor lead angle see Fig. 2
L_e	fighter climb angle see Fig. 2
L_e^*, L_a^*	ideal values of L_e and L_a for missile launch
$\underline{M}$	vector miss distance T seconds from now
M_x	component of $\underline{M}$
M_y	component of $\underline{M}$
M_z	component of $\underline{M}$
$\underline{R}$	position of fighter relative to target
R	slant range target to fighter
R_H	horizontal component of $\underline{R}$
T	time-to-go see equations (8 and 8a)
T_h	thrust of fighter
t_f	time of flight of missile

$\underline{V_f}$ fighter velocity relative to ground

V_f fighter speed

V_{fo} initial fighter speed

$\underline{V_t}$ target velocity

V_t target speed

$\underline{V_m}$ mean missile velocity

V_m mean missile speed

W weight of the fighter

XYZ coordinate system Fig. 2

X horizontal and is parallel to R_H

Y is normal to X and is in the same horizontal plane

Z is vertically downward

$X_f\ Y_f\ Z_f$ coordinate system (wind axes)

X_f is in the direction of the fighter velocity

Z_f is normal to X_f and is in the same vertical plane

Y_f is normal to X_f and Z_f

For this study the fighter axis is assumed to be along X_f

X_f', Y_f', Z_f' as X_f, Y_f, Z_f but rotated about OX_f' until OY_f' is in the plane of the wings

α fighter angle of attack

δ_a approx. component of heading error

δ_e approx. component of heading error

δ^x heading error at launch

Δh altitude difference - target to fighter

ΔV average incremental missile velocity

ϵ_a, ϵ_e components of angular heading error

ϵ antenna elevation gimbal deflection

θ antenna azimuth gimbal deflection

ϕ fighter bank angle

ω_a components of fighter angular velocity

ω_e components of fighter angular velocity

4.0 ANALYSIS OF THE INTERCEPTION PROBLEM

4.1 Geometry

Figure 2 shows the situation during an attack and defines some symbols and reference axes.

$$\dot{\underline{R}} = \underline{V_f} - \underline{V_t} \tag{1}$$

This vector equation may be resolved into three components

$$\dot{R}_H = V_t \cos A - V_f \cos L_e \cos L_a \qquad \text{(Fig. 28)} \tag{2}$$

$$\dot{A} = \frac{1}{R_H}\left\{ V_f \cos L_e \sin L_a - V_t \sin A \right\} \qquad \text{(Fig. 29)} \tag{3}$$

$$\dot{\Delta}_h = -V_f \sin L_e \qquad \text{(Fig. 28)} \tag{4}$$

If a lead collision course is desired, miss is defined by

$$\underline{M} = \underline{R} + \dot{\underline{R}}\, T + \underline{F} \qquad \text{(see Fig. 3)} \tag{5}$$

This equation is resolved into three components:-

$$M_x = (V_f T + F) \cos L_e \cos L_a - V_t T \cos A - R_H \qquad \text{(Fig. 28)} \tag{6}$$

$$M_y = V_t T \sin A - (V_f T + F) \cos L_e \sin L_a \qquad \text{(Fig. 30)} \tag{7}$$

$$M_z = \Delta h - (V_f T + F) \sin L_e \qquad \text{(Fig. 31)} \tag{8}$$

Time-to-go condition is determined by $M_x = 0$ (Fig. 28) (9)

In an aircraft the basic fire control equations are handled in radar coordinates so that in practice, time-to-go would be defined by equating the component of miss along the line of sight to zero.

i.e. $\underline{M} \cdot \underline{R} = 0$ (10)

The effects of this difference in defining time-to-go are discussed below.

The scheme outlined above (equations 1 to 9) is discussed in more detail in "A General Description of the Universal Computer" Ref. 1.

4.2 Heading Error

To find the ideal heading, consider equations (6), (7), (8). If T, L_e, L_a are replaced by T*, L_e*, and L_a* which correspond to zero miss distance, then

$$0 = (V_f T^* + F) \cos L_e^* \cos L_a^* - V_t T^* \cos A - R_H \tag{11}$$

$$0 = V_t T^* \sin A - (V_f T^* + F) \cos L_e^* \sin L_a^* \tag{12}$$

$$0 = \Delta h - (V_f T^* + F) \sin L_e^* \tag{13}$$

Let $T^* = T + t$, $L_e^* = L_e + \epsilon_e$, $L_a^* = L_a + \epsilon_a$

Substitute these values in equations (11) (12) and (13) and solve for ϵ_a and ϵ_e from (6) (7) (8), (11) (12) and (13) simultaneously. This solution is simplified by assuming ϵ_a, ϵ_e and t are small (as they must be for a successful attack). Hence products of these quantities are neglected and $\cos L_e^* \doteq \cos L_e - \sin L_e \epsilon_e$

$$\sin L_e^* \doteq \sin L_e + \cos L_e \epsilon_e$$

L_e* and L_a* are the ideal heading components and hence ϵ_e and ϵ_a are the heading error components.

$$\epsilon_e = \frac{M_z \left(\cos L_a + \frac{R_H \dot{A}}{\dot{R}_H} \sin L_e\right) + M_y \sin L_a \frac{\dot{\Delta h}}{\dot{R}_H}}{(V_f T + F)\left\{\cos L_e \cos L_a + \frac{R_H \dot{A}}{\dot{R} H} \cos L_e \sin L_a - \frac{\dot{\Delta h}}{\dot{R} H} \sin L_e\right.} \tag{14}$$

$$\epsilon_a = \frac{M_y \left(\cos L_e - \frac{\dot{\Delta h}}{\dot{R} H} \cos L_a \sin L_e\right) + M_z \sin L_e (\sin L_a}{\cos L_e (V_f T + F)(\cos L_e \cos L_a + \frac{R_H \dot{A}}{\dot{R} H} \cos L_e \sin L_a + \frac{R_H A}{\dot{R} H} \cos L_a)} \tag{15}$$

$$- \frac{\dot{\Delta h}}{\dot{R} H} \sin L_e$$

The heading error components are used for two different purposes in the study.

1. to provide steering information during the attack

2. to judge the success or failure of an attack by comparing the actual heading error at launch with the error which the missile guidance system can compensate.

4.3 Aircraft Performance

Assuming thrust and drag act along the velocity vector, from the geometry of Fig. 4.

$$\dot{V}_f = \frac{T_h - D}{W} g - g \sin L_e \qquad \text{(Fig. 34)} \qquad (16)$$

$$V_f \omega_a = \frac{L}{W} g \sin \phi \qquad \text{(Fig. 33)} \qquad (17)$$

$$V_f \omega_a = \frac{L}{W} g \cos \phi - g \cos L_e \qquad \text{(Fig. 33)} \qquad (18)$$

Avro estimates of performance Refs. 2, 3, 4 are the source of the information from which thrust and drag functions were mechanised. The mechanisation is described in Ref. 5.

Changes in the altitude of the fighter are determined by

$$\dot{L}_e = \omega_e \qquad \text{(Fig. 31)} \qquad (19)$$

$$-\dot{L}_a = \omega_a \sec L_e - \dot{A} \qquad \text{(Fig. 30)} \qquad (20)$$

If sufficient lift is available

$$\omega_a = -K \delta_a \qquad \text{(Fig. 30)} \qquad (21)$$

$$\omega_e = K \delta_e \qquad \text{(Fig. 31)} \qquad (22)$$

where

$$\delta_a = \frac{M_y}{V_f T + F} \qquad \text{(Fig. 30)} \qquad (23)$$

and

$$\delta_e = \frac{M_z}{V_f T + F} \qquad \text{(Fig. 31)} \qquad (24)$$

If $\dot{R}_H$ is large compared with $R_H\dot{A}$ and $\dot{\Delta h}$, equations (14) and (15) give

$$\epsilon_e = \frac{M_z}{(V_f T + F)\cos L_e}$$

$$\epsilon_a = \frac{M_y}{(V_f T + F)\cos L_e \cos L_a}$$

In "A General Description of the Universal Computer", Hughes Aircraft Co. suggest that steering should be controlled by δ_a and δ_e instead of ϵ_a and ϵ_e. This is equivalent to changing the gain of the steering demand loops. The steering is designed to make M_y and M_z approach zero so that the aircraft is steered onto a lead collision course, but the steering demands are not quite proportional to the angular heading errors.

In the case where insufficient lift is available for equations (21) and (22)

$$\omega_a = -K'\delta_a \qquad \text{(Fig. 30)} \qquad (25)$$

$$\omega_e = K'\delta_e \qquad \text{(Fig. 31)} \qquad (26)$$

where K' is determined by

$$-V_f K'\delta_a = \frac{L_{max}}{W} \cdot g \sin \phi \qquad \text{(Fig. 33)} \qquad (27)$$

$$V_f K'\delta_e = \frac{L_{max}}{W}\, g \cos \phi - g \cos L_e \qquad \text{(Fig. 33)} \qquad (28)$$

L_{max} is instrumented as a function of Mach no. and pressure, Fig. 34 Ref. 2. Pressure is assumed to be a simple function of altitude, Fig. 32.

4.4 Launch Zone

It is assumed that the missile flies a distance F relative to the fighter (in the direction of the fighter velocity at launch) in a time of flight t_f. F and t_f have been assumed constant over a wide range of circumstances.

The approximate heading error components δ_a and δ_e are not used but actual values of L_a and L_e are compared with ideal values L_a^* and L_e^* determined from equations (11) (12) and (13), Fig. 30 and 31) the total heading error being approximated by

$$\delta^* = \left\{(L_e - L_e^*)^2 + (L_a - L_a^*)^2\right\}^{1/2} \qquad \text{Fig. 36)} \qquad (30)$$

This is compared with a standard allowable error given in Fig. 20.

4.5 Radar Antenna Deflections (Fig. 5)

The azimuth and elevation gimbal deflections of the AI radar antenna are determined from

$$R \cos\theta \cos\epsilon = (R_H \cos L_a \cos L_e + \Delta h \sin L_e)\cos\alpha - \left\{(R_H \cos L_a \sin L_e - \Delta h \cos L_e)\cos\phi - R_H \sin L_a \sin\phi\right\}\sin\alpha \quad (31)$$

$$R \sin\theta \cos\epsilon = R_H \sin L_a \cos\phi + (R_H \cos L_a \sin L_e - \Delta h \cos L_e)\sin\phi \quad (32)$$

$$R \sin\epsilon = \left\{(\Delta h \cos L_e - R_H \cos L_a \sin L_e)\cos\phi + R_H \sin L_a \sin\phi\right\} \cos\alpha - (R_H \cos L_a \cos L_e + \Delta h \sin L_e) \sin\alpha \quad (33)$$

See Fig. 35. From the LHS of these expressions θ and ϵ are obtained (Fig. 36). They are compared with their limits during each flight and values at launch are checked to determine whether the missile can see the target or is blinded by the airframe. (See Fig.7)

5.0 AN ASSESSMENT OF THE ACCURACY OF THE REAC STUDY

In order to fit the problem to a 120 amplifier computer it was necessary to make use of some trigonometric approximations and some other simplifications.

The effects of these approximations are discussed below.

The errors which have been calculated are not corrections to be applied to REAC results. Generally they are order of magnitude calculations which have been computed from the worst cases which are likely to occur.

Errors due to approximations in vertical trigonometry are computed for attacks from 40,000 ft.against a target at 60,000 ft.

5.1 Geometry

In mechanising the geometrical equations (2), (3) and (4), L_e is substituted for $\sin L_e$ and unity for $\cos L_e$ as the angle L_e is usually small. Hence the REAC equations are

$$\dot{R}_H = V_f \cos A - V_f \cos L_a \qquad 2(a) \text{ Fig. } 28$$

$$\dot{A} = \frac{1}{R_H}\left\{V_f \sin L_a - V_t \sin A\right\} \qquad 3(a) \text{ Fig. } 29$$

$$\dot{\Delta h} = -V_f L_e$$

If L_e is large, these equations give an optimistic picture of the aircraft's ability. In particular it covers horizontal distances as though its full velocity were in the horizontal plane. The error is shown in Figs. 9 and 10. This will result in misplacement of fall-back, minimum-fighter-velocity and maneuver barriers.

These effects will be discussed in more detail below, as the barriers are also affected by approximations in the other geometrical equations. Equations (6), (7), (8) define the miss distance in a lead collision attack. In the computer set-up time-to-go is defined by $M_x = 0$ (equ. 9) instead of $\underline{M}.\underline{R} = 0$ (equ. 10) as it would be in the aircraft computer working in radar coordinates.

$$\underline{M}\cdot\underline{R} = M_x R_H + M_z \Delta h \qquad (10a)$$

$$= R_H^2 + R_H V_t T \cos A - R_H (V_f T + F) \cos L_e \cos L_a + (\Delta h)^2 - \Delta h (V_f T + F) \sin L_e$$

$$= R \left\{ R + \frac{R_H}{R} \left(V_t T \cos A - \left\{ V_f T + F \right\} \cos L_e \cos L_a \right) - \frac{\Delta h}{R} (V_f T + F) \sin L_e \right\}$$

If Δh is small compared with R_H then 10a becomes $R_H M_x = 0$ ie $M_x = 0$ defines time-to-go quite accurately. In addition, the steering is designed to make M_z approach zero, so that once the interceptor is on course $M_z \Delta h$ is zero and hence $\underline{M}.\underline{R} = 0$ so that both systems give the same answer for time-to-go. The vertical heading error is given approximately by

$$\epsilon_e = \frac{M_z}{(V_f T + F) \cos L_e}$$

If near the end of the attack M_z is not small, the launch zone will be erroneously defined owing to the error in computing time-to-go but the attack will be a failure owing to the excessive heading error.

In the equations defining miss distance, it is assumed that L_e is a small angle and the equations which are mechanised are

$$\frac{l}{T} = \frac{1}{R_H} \left\{ \left(V_f + \frac{F}{T} \right) \cos L_a - V_t \cos A \right\} \qquad 6(a) \text{ Fig. } 28$$

$$\frac{M_y}{T} = V_t \sin A - \left(V_f + \frac{F}{T} \right) \sin L_a \qquad 7(a) \text{ Fig. } 30$$

$$\frac{M_z}{T} = \frac{\Delta h}{T} - \left(V_f + \frac{F}{T} \right) L_e \qquad 8(a) \text{ Fig. } 31$$

The REAC layout is a direct analogue of these equations.

In one series of problems, the launch zone was defined by time-to-go T equals a constant corresponding to a constant time of flight for the missile. In the REAC study, for a particular value of fighter speed, this is a cylindrical surface instead of a spherical one as the climb angle information in equation (6) does not appear in equation (6(a)). For climbing attacks from long range the error involved in this approximation is very small but it was felt that a study should be carried out to determine its effects from shorter ranges.

This study relied on the fact that while vertical equations of motion are approximate, the equations covering motion in the horizontal plane are accurate. The pressure function was kept constant and the components of the aircraft's weight were disconnected. A number of interceptions were carried out for an initial course difference of 180°, parallel courses 20 K ft. apart and various ranges. Corresponding runs were carried out in the vertical and horizontal planes. The runs were terminated at T = 8 secs. Values of heading error, climb angle (or course difference) and range were recorded.

In the horizontal plane, time-to-go is defined by

$\underline{M}.\underline{R} = 0$ as $\Delta h = 0$ (see equ. 10(a).

In the vertical plane, this is not so. In the REAC further approximations are made in computing T.

Hence this study is a comparison between the behaviour of an aircraft whose computer works on radar coordinates and the REAC simulation.

Results are shown in Fig. 11 - Trajectories; Fig. 12 - Final Heading Error and Fig. 13 Final Climb Angle. Using the results of this section, some calculations were made on the location of minimum velocity and fall back barriers. The results of these calculations are given in Figs. 14 and 15.

In mechanising equations (23) (24) (25) (26) on the computer $\frac{M_y}{T}$ and $\frac{M_z}{T}$ to a scale factor of 0.2778 have maximum values of 100 v (Fig. 30 & 31). Hence $\frac{M_y}{T}$ and $\frac{M_z}{T}$ have maximum values of 360 feet/sec. For an interceptor speed of M 2.0 this corresponds to a heading error of 10.6° at zero aspect. If the actual error is greater than this, the aircraft behaves as if the error were 10.6°. If the azimuth error were 45° and the climb angle error were 15°, instead of the aircraft banking to reduce these proportionally, it banks to reduce them equally so that in practice, near placement zone boundaries the aircraft tends to correct elevation errors before azimuth errors. Hence the aircraft will initially be banked to a smaller angle than it should be and then when the elevation errors have been almost corrected, it pulls full g's in azimuth and banks to a steeper angle than it would have in the absence of the limits on $\frac{M_y}{T}$ and $\frac{M_z}{T}$ This process produces pessimistic look angle barriers especially for course differences near 180°.

For smaller initial course differences the look angle barriers are closer to the ideal approach line so this effect is reduced. The results are shown in Fig. 16.

Look angle barriers are sensitive to bank and hence to the sequence in which vertical and horizontal errors are corrected. Generally it seems preferable to correct horizontal errors at a greater rate than vertical errors.

This limitation is not so much an error in computing the problem as a request by the navigation computer to fly a slightly different trajectory.

5.2 Aircraft Performance

In the section dealing with the geometry of the interception it was shown that approximations in some of the trigonometric functions give rise to an optimistic picture of the velocity of the aircraft for large climb angles. Similar approximations give rise to a slightly pessimistic picture of the aircraft acceleration.

i.e. $\dot{V}_f = \frac{Th - D}{W} g - g L_e$ 16(a) Fig. 34

$V_f \omega_a = \frac{L}{W} g \sin \phi$ 17 Fig. 33

$V_f \omega_e = \frac{L}{W} g \cos \phi - g$ 18(a) Fig. 33

are the equations which are mechanised. In equations (16(a)) and 18(a) the component due to the weight of the aircraft is too large when the aircraft is climbing and in equation 20(a) $-L_a = \omega_a - \dot{\lambda}$, the effective turn rate of the aircraft is smaller due to the approximation.

The Avro thrust and drag information is mechanised in the following way.

It is assumed that thrust and drag can be represented by

$$T_h - D = \left\{\frac{T_h - D_o}{P_o}\right\} P_o - K_1 L - \frac{\mathcal{J} L^2}{P_o} \qquad \text{Fig. 34}$$

where $\frac{T_h - D_o}{P_o}$, K_1, and $\mathcal{J}$ are functions of Mach number only.

The accuracy of this approximation for an aircraft flying at 50,000 feet is shown in Fig. 6. Errors include inaccuracies in reproducing $\frac{(T_h - D_o)}{(P_o)}$ K_1 and $\mathcal{J}$.

To give some idea of the error caused by substituting L_e for sin L_e in equation 16(a) a calculation has been carried for the case when L_e final has its maximum value = 35°. Time of engagement = 20 seconds, mean fighter speed = 1400 ft/sec.

Error in final speed	= 62 ft/sec	i.e.	4·5%
Error in mean speed	= 16 ft/sec		1%

5.3 Launch Zone

In the CARDE model of CF-105 interceptions, the attack is stopped when time-to-go is equal to the time of flight of the missile. The ultimate success or failure of the attack depends on whether the orientation of the aircraft at this instant will ensure that the missile ultimately kills the target. This is necessarily a complex problem and has been the subject of a separate study. The permissible heading error of the missile at launch, that is the maximum heading error that the missile guidance can correct, depends on many interacting parameters, target and interceptor speed, course difference, altitude, range, etc.

5.4 Ideal Heading Calculation

This is the heading which would result in a successful attack if the missile were not guided. If the target flies in straight line at a constant speed, this calculation is quite straight forward. When the target is maneuvering, the ideal heading is computed assuming that the maneuver ceases when the missile is launched. The error in making this assumption can be compensated by permitting a smaller deviation from ideal heading in the guided missile. (This presumes that the target is maneuvering to make interception more difficult).

The heading error is computed by measuring the actual heading and comparing it with the ideal heading. See equations 6, 7, 8, 9 and 11, 12, 13.

5.5 Calculating of the Components of Heading Error

Changes in heading are produced by the aircraft's answering steering demands accurately as long as sufficient lift is available and otherwise using maximum available lift to turn in answer to steering demands.

The errors which result in steering demands are computed in the $\frac{M_y}{T}$ and $\frac{M_z}{T}$ circuits. The ideal heading is computed at the end of each run by means of the same equipment that computes the steering errors and is found by substituting the values of the heading components which correspond to zero error.

Some approximations are made in computing $\frac{M_z}{T}$, but as the same equipment is used in computing L_e^* (ideal climb angle) no error is introduced due to inconsistency.

Fig. 18 shows the different launch zones which result from different definitions for time-to-go.

Fig. 19 shows the effect of this on the maneuver barrier near the ideal approach line.

Fig. 20 shows the variation in permissible heading error with altitude.

The launch zone is mechanised in Fig. 37. Both range and time-to-go criteria for launch may be employed.

5.6 Heading Error Calculation

The heading of the interceptor may be defined by its direction cosines in the XYZ axis system (see Fig. 2). Consider a point r feet along the fighter velocity vector. If the interceptor is considered as the origin. The coordinates of point are

$$(r \cos L_e \cos L_a, \; - r \cos L_e \sin L_a, \; - r \sin L_e)$$

Hence the direction cosines of the heading are

$$(\cos L_e \cos L_a, \; - \cos L_e \sin L_a, \; - \sin L_e)$$

with respect to XYZ axes. The direction cosines of the ideal heading are

$$(\cos L_e^* \cos L_a^*, \; - \cos L_e^* \sin L_a^*, \; - \sin L_e^*).$$

The angle between the ideal and the actual heading is given by

$$\begin{aligned} \cos \delta^* &= \cos L_e \cos L_a \cos L_e^* \cos L_a^* + \sin L_a \cos L_e \sin L_a^* \\ &\quad \cos L_e^* + \sin L_e^* \sin L_e \\ &= \cos L_e \cos L_e^* \cos (L_a - L_a^*) + \sin L_e \sin L_e^* \\ &= \cos (L_e - L_e^*) \cos (L_a - L_a^*) + \sin L_e \sin L_e^* \\ &\quad (1 - \cos (L_a - L_a^*) \end{aligned} \qquad \text{--- 30(a)}$$

e.g. when $L_e = 30^\circ$, $L_e^* = 40^\circ$, $(L_a - L_a^*) = 10^\circ$

$\cos \delta^* = .9701 + .0049$

If the first term only is used, $\delta^* = 14.05^\circ$

If both terms are used $\delta^* = 12.83^\circ$

In the REAC approximation, $\delta^* = \left[(L_a - L_a^*)^2 + (L_e - L_e^*)^2 \right]^{1/2}$

In this case $\delta^* = 14.14^\circ$

This is very close to saying $\cos \delta^* = \cos (L_e - L_e^*) \cos (L_a - L_a^*)$

The major part of the error is in neglecting the term

$$\sin L_e \sin L_e^* \left\{ 1 - \cos (L_a - L_a^*) \right\}$$

The effect of this error is shown in Fig. 17.

The component of heading error owing to changes in angle of attack with altitude and lift is neglected and changes in the attitude of the missile at launch are neglected. The ideal heading is computed assuming the missile flies along the fighter's velocity vector as it will tend to weather cock into this direction.

The ideal heading is computed neglecting any evasion by the target subsequent to launching the missile. The effects of this assumption are discussed below.

5.7 Effect of Neglecting Target Evasion After Launch

Consider the specific case of M2.0 target evading with 1.25 g load factor i.e. .75 lateral g's

Rate of turn of target $r_t = \frac{.75g}{V_t} = .712^\circ/\text{sec.}$

in 8 seconds time of flight it turns 5.7°.

Average missile velocity is M2.875

Hence missile has to turn $5.7 \frac{V_t}{V_m} = 3.96^\circ$

In the case of an attack from 40K ft against a 60K ft target from the ideal approach line, heading error permitted at launch equals 22.0°. See Fig. 19.

New heading error at launch is given by $\delta^* = \sqrt{22.6^2 + 3.96^2} = 22.9^\circ$

This change in heading error corresponds to a change in initial fighter range of 300 ft as the slope of the heading error versus initial range curve has a slope of 1° per 1000 ft for heading errors near 22°. (See Fig. 12)

In the case of a coaltitude attack at 60 K feet, the change in heading error due to target evasion is in the same plane as the heading error due to initial placement. The allowable error at this altitude is only 8° so that if an error of 4° is introduced by target evasion, the heading error at launch should be only 4°. (Initial range for 4° heading error) - (Initial range for 8° heading error) = 2000 feet, as the slope of the horizontal heading error curve at this point is 500 feet per degree.

5.8 Look Angle Barriers and the Axis Transformation

Because of the limits on the azimuth and elevation gimbal deflections it is necessary to know the angular position of the target with respect to the fighter axes throughout an attack.

The axis system (X_f', Y_f', Z_f') is shown in Fig.5 . X_f' is measured along the fighter axis, Y_f' is in the plane of the wings normal to X_f' and Z_f' is normal to X_f' and Y_f'.

When the aircraft flies with zero climb angle, zero bank angle and zero angle of attack, the coordinates of the target in terms of gimbal deflection angles θ and ϵ are given by

$$R \cos\theta \cos\epsilon = R_H \cos L_a$$

$$R \sin\theta \cos\epsilon = R_H \sin L_a$$

$$R \sin\epsilon = \Delta h$$

When the aircraft flies with climb angle L_e, bank angle ϕ and angle of attack α, the appropriate equations are (31) (32) and (33). These are mechanised on the REAC assuming that the angles L_e and α are small.

$$R \cos\theta \cos\epsilon = (R_H \cos L_a + \Delta h\, L_e) - \left\{(R_H \cos L_a\, L_e - \Delta h) \cos\phi - R_H \sin L_a \sin\phi\right\}\alpha \qquad 31(a)$$

$$R \sin\theta \cos\epsilon = R_H \sin L_a \cos\phi + (R_H \cos L_a\, L_e - \angle h) \sin 0 \qquad 32(a)$$

$$R \sin\epsilon = (\Delta h - R_H \cos L_a\, L_e) \cos\phi + R_H \sin L_a \sin\phi - (R_H \cos L_a + \Delta h\, L_e) \qquad 33(a)$$

The circuit on Fig. 35, "Axis Transformation I" produces the right hand sides of these equations.

"Axis Transformation II" in Fig. 36 obtains ϵ and θ from $R \cos\theta \cos\epsilon$, $R \sin\theta \cos\epsilon$, $R \sin\epsilon$. θ and ϵ are continuously displayed and compared with their limits.

For the latest series of problems the look anglelimits were taken as $\theta = \pm 70^\circ$, $\epsilon = 75^\circ$ and -45°
The missile cannot be launched successfully unless

$$\epsilon < 5.0^\circ + |0.241|\ \theta^\circ.$$

Fig. 7.

5.9 Errors in the Axis Transformation System

The errors may be divided into two categories - random errors and systematic errors. The random errors include amplifier and servo noise and the systematic errors are those due to phase shift, frequency response and non-linearity in the amplifiers and servos. The first two systematic errors may be reduced to any desired level by time scaling the problem, since the rate at which the computer runs the problem may be chosen.

In this problem some additional systematic errors are present. The bank angle α is derived from the velocity of the aircraft and the value of $\frac{L}{P_o} \cdot \frac{\alpha L}{P_o}$ is a function of Mach number alone see Ref. 13. Fig. 21 shows data deduced from this reference with the REAC approximation. The errors are small compared with other errors in the system.

Owing to a shortage of computing equipment, it was necessary to make some trigonometrical approximations. The angle of attack α is less than $16^{\circ}.20'$ in the range M0.8 to M2.0 and the elevation angle L_e is small at the long and medium ranges where look angle boundaries occur. Hence it was decided to make the approximations $\sin \alpha = \alpha$, $\cos \alpha = 1$ and $\sin L_e = L_e$, $\cos L_e = 1$.

A series of calculations were carried out for the case $\triangle h = 20{,}000$ ft, $R_H = 50{,}000$ ft, Bank angle $\phi = 60^{\circ}$, lead angle $L_a = 40^{\circ}$, angle of attack $\alpha = 0, 5^{\circ}, 10^{\circ}, 15^{\circ}$ and elevation angle $L_e = 0, 10^{\circ}, 20^{\circ}, 30^{\circ}, 40^{\circ}$.

These are typical figures for the situation where errors in the axis transformation will be important. Look angle failures result from two main effects.

1. Look angle failure due to the proximity of a fall back barrier. When $\dot{R}$ becomes positive $1/T$ goes negative and the control demands are reversed. The fighter proceeds to steer away from the target until it gains sufficient speed to make $\dot{R}$ negative again. Before this happens, the target may be lost on the fighter's radar.

2. Look angle failure due to a large value of lead angle. With the AI radar look angle limits that were used in the last series of problems, the most common look angle failure is $\epsilon < -45^{\circ}$. If the bank angle is large and negative say $\epsilon \doteq -(\alpha + L_a)$. If α is 15° and $L_a = 40^{\circ}$, a bank angle of only 50° ($\equiv$ 1.2 lateral g's) is sufficient to ensure a look angle failure.

In most of the look angle failures due to fall back, a change in look angle limits or a small error in the calculation of look angle components will not affect the position of the barrier. The exception to this statement is when recovery from fall back is possible but even here, the change in the barrier position is quite small even when the fighter has a potential speed advantage.

Hence errors in look angle calculation need only be considered in the case of look angle failure due to excessive lead angle.

The error due to the range of values of α is quite small compared with the error due to the range of values of L_e since α max = 16°.20'. Figs. (22 & 23) give a plot of errors in ϵ for different initial fighter positions. In this latter it is assumed that initially the fighter is flying level, banks to correct equal horizontal and vertical errors and goes out on look angle just before it reaches its steady value of L_e.

5.10 Dynamic Lags in the System

5.10.1 Spurious Dynamic Lags

In some parts of the system, the equations give rise to a potentially unstable REAC layout. This often occurs when the REAC is asked to perform essentially algebraic operations. When groups of simultaneous equations are solved on the REAC, closed loops with a gain around the loop numerically greater than unity are stable if the gain is negative. However, incidental phase shift in amplifiers and servos will often result in instability.

Any such circuit which has a finite negative loop gain at low frequencies and is unstable due to phase shift at higher frequencies may be stabilised by introducing a simple RC low pass filter. In the REAC, this means placing a capacitor in parallel with the feedback resistor.

The gain of a summer with a shunt feedback capacitor C is given by

$$\frac{E_{out}}{E_{in}} = \frac{1}{\sqrt{(1 + 4\pi^2 f^2 C^2 R_f^2)}}$$

and the phase shift is $\tan \psi = -2\pi fRC$. Any loop can can be made stable by choosing C sufficiently high that the gain around the whole loop is less than unity before the phase shift is 180°.

This form of stabilisation was necessary in the K'/K loop and in the circuit which derives L and ϕ from L cos ϕ, L sin ϕ. (no resolver servo was available for this purpose).

The lag introduced by such a method may produce undesirable effects. One way to check this is to double the size of the stabilising capacitors (which should of course be the smallest consistent with a stable set-up). If the performance changes significantly it means that the problem is being run too fast and the scale must be changed.

5.10.2 Real Lags

No attempt has been made to simulate the response time of the pilot or autopilot and time delays in the system .

The response of the aircraft to control demands was assumed to be immediate. This assumption removes two awkward difficulties and introduces no serious defect.

(i) Detailed information on the response time was not available.

(ii) Had an attempt been made to simulate this and other results of the dynamics of the aircraft itself, the problem would have been beyond the scope of CARDE'S 120 amplifier computer. It was argued that the time delays involved would be small compared with the duration of the attack and at the same time we would be providing an ideal which the aircraft would approach. Namely, the optimum achievement that the aerodynamic performance can produce.

In particular, the gain of the steering system is made very high and a limit is placed on allowable lift. In practice, this high value would probably result in instability in the aircraft owing to dynamic lags in the system.

Figure 24 illustrates the effect of a change in the gain of the steering system. The main consequence of such a change would be a shift in maneuver barriers due to a slower approach to the ideal heading.

6.0 SNAP-UP ATTACKS

The model was originally designed to fly lead collision and lead pursuit attacks but was easily adapted to cope with snap-up attacks. The aircraft flies a lead collision course in which the vertical steering error is disconnected until some predetermined time-to-go. See Fig. 39. From this instant the aircraft climbs steeply flying a normal lead collision course until it reaches the launch zone.

A general study of snap-up attacks was carried out and several important points were brought out. Some of these are given below.

The time-to-go at snap-up which was chosen for this first study was some 20% larger than the time-to-go corresponding to the minimum successful range. This was to prevent maneuver failures due to errors in time-to-go calculation arising from incorrect heading etc.

Look angle barriers (not directly associated with fall-back) at medium and long ranges are not affected by small changes in snap-up time-to-go. This is because the aircraft is flying level at the time when it comes close to failure and subsequent introduction of new steering information is of no importance.

Fall-back and minimum velocity barriers are affected to a "second order" only by small changes in snap-up time-to-go as changes in altitude rather than actual trajectories are significant.

The transition from look-angle, full-back and minimum velocity barriers to maneuver barriers and the outer-parts of themaneuver barriers are dependent on the time-to-go when snap-up occurs. Generally, in an attack where snap-up gives a larger placement zone than a climbing attack the placement zone increases the smaller the value of time-to-go which is chosen for the initiation of snap-up.

This process continues until the aircraft has insufficient time to climb to a suitable angle for a successful attack.

The ideal snap-up time-to-go then is the time which corresponds to this change over from increasing success to complete failure, plus a suitable safety factor to prevent accidental placement in the failure region.

Snap-up time-to-go varies with the launching requirement of the missile and the speed and altitude of the interceptor and the altitude of the target (the initial fighter speed was M2.0 in all cases studied).

It is independent of the initial course difference between interceptor and target. Fig. 25 shows the effect of a change in time-to-go at snap-up.

6.1 Circuit Changes to Include Snap-up as a Possible Mode of Attack

$\frac{K'M_z}{T}$ to ω_e when time-to-go was less then the standard value of the problem initial conditions.

In an attack from long range, azimuth errors are usually sufficiently small that $K' = K$ just before snap-up. Owing to the lag in the servo loop ω_e initially corresponds to $K\frac{M_z}{T}$ which in turn $\frac{K'}{K}$ corresponds to a much faster turn rate than the aircraft is capable of. Hence an additional overriding limit of $V_f\omega_e = 3$ g was included.

When the interceptor flies at 40,000 feet the maximum load factor at all speeds is 4 g. For vertical maneuvering, if 1 g is reserved for the weight of the aircraft, 3 g remains for going into a climb.

This circuit gives a slightly optimistic picture of the ability of the interceptor at height greater than 40,000 feet or when there is a residual azimuth error (when less than 3 g's are available for climbing). However, it was found in practice that the exact value of this limit is not critical as the K'/K servo loop quickly takes over. It is merely necessary to prevent the initial large overshoot which would otherwise occur.

7.0 CONCLUSIONS

The approximations which have been made in the REAC simulation have a small effect on placement probability.

Fig. 26 shows the effects of the trigonometric approximations on the placement zone and in Fig. 27 these are reduced to placement probability. The effects of errors in computing ϵ are quite small as look angle barriers do not occur at the short ranges where the errors are large.

Similarly the error in computing fall back and minimum velocity barriers is small for the ranges at which these barriers are found.

The error in computing maneuver barriers is quite small. The error shown is that due to approximating in the calculation of time-to-go but not in the definition of time-to-go.

i.e. assuming time-to-go is defined from $M_x = 0$

The main difference involved is due to the limit on M_y - this is more like another mode of attack in which heading errors are not corrected proportionally.

In snap-up attacks the errors are even smaller as the aircraft flies level for most of the attack.

8.0 OUTPUT EQUIPMENT

The initial fighter position with respect to the target and its subsequent motion in target coordinates are displayed on a plotting table to a scale of 10,000 feet per centimetre. Range of up to 400,000 feet may be displayed.

The target angular position relative to the fighter axis with AI limits and missile blinding limits is shown on a smaller plotting table to a scale of 20° per inch.

In addition to these, a four channel recorder (and until recently an 8 channel recorder) recorded the more important problem variables for points along the boundary between the hit and miss zones.

Boundaries are defined by marking the initial interceptor positions which correspond to a change over from success to failure.

For convenience in operating, a remote control system is included. (See Fig. 38).

This figure also shows the relays which are used to enable L_e* and L_a* to be computed at the end of each run.

9.0 ACKNOWLEDGEMENTS

The 3D REAC study has been carried out by a large number of people over a period of some two years. The initial phases of the problem including the design of the REAC layout were done by C.J. Wilson and G.R. McCully.

Subsequent work on the computer has been carried out by J.F. Blansche, P.T. Caden, F.F. Van Humbeck and C.W. Lester.

In a problem of this type considerable data reduction is necessary. Acknowledgement should be made to the "G" Wing Data Reduction Lab. particularly B. Thibault and to Miss J. O'Donnell and Miss C. Bouchard.

10.0 REFERENCES

1. General Description of the Universal Computer TM-339 Report No. 479A-11-F2 - Hughes Aircraft Corp. CONFIDENTIAL

2. AVRO report CF-105 Periodic Performance Report No. 9 (Nov/Dec 1956) Report P/Aero Data/74 Issue II SECRET

3. AVRO report CF-105 Periodic Performance Report No. 10 (Dec 1956) SECRET

4. AVRO Report No. P/Power/87 Iroquois Corrected Thrust, Two Engines, After-burners Lit, Rematched Compressors Variable Ejector. CONFIDENTIAL.

5. Internal Memorandum from D.W. Pounder to C.J. Wilson file S/N-47-3 dated 22nd Feb. 1957 on CF-105 Aerodynamics. SECRET

6. Internal Memorandum on file No. S/N-47-3 dated July 12, 1956 to R.S. Mitchell from F. Chown "A 3D Placement Study". SECRET

7. Internal Memorandum on File No. S/N-47-3 dated Sept. 24/56 to R.S. Mitchell from C.J. Wilson "A REAC Set-up for Solutions of 3-D Placement Problems". SECRET

8. Internal Memorandum on file No. S/N-47-3 dated Oct. 4, 1956 to C.J. Wilson from K. Acton on "Simulation of Performance of CF-105 on REAC" SECRET

9. Internal Memorandum on file No. S/N-47-3 dated Oct. 31, 1956 to C.J. Wilson from D.W. Pounder on CF-105 3D Placement Study. SECRET

10. Internal Memorandum on file CARDES 9736-21 dated 27 Sept. 1957 to C.J. Wilson from J.A. Ockenden "Fire Control Studies - AI Navigation" SECRET.

11. Internal Memorandum on file S/N-47-3 dated 1st March 1957 to R.S. Mitchell from A.I. Matheson. "Summary on RCA Quarterly Progress Report # 1 (Astra 1) SECRET.

12. CF-105 Missile Blinding - CARDE Tech. Letter N-47-8 p. 33 SECRET

13. AVRO Report P/Control/78 dated July 1955 - CF-105 Longitudinal Control. SECRET.

14. CARDE Tech. Letter N-47-8 "First Quarterly Report on CF-105 Weapon System Assessment" Appendix G SECRET

15. CARDE Tech. Letter N-47-12 "Second Quarterly Report on CF-105 Weapon System Assessment" Appendix 'D' SECRET

16. CARDE Tech. Letter N-47-18 "Third Quarterly Report on CF-105 Weapon System Assessment" Appendix 'G' SECRET

17. CARDE Tech. Letter 1012/57 "Fourth Quarterly Report on CF-105 Weapon System Assessment" Appendix 'A' SECRET

18. CARDE Tech. Letter 1091/58 "Fifth Quarterly Report on CF-105 Weapon System Assessment" Appendix 'A' SECRET

Figure 1 - CF-105 Block Diagram Corresponding to REAC Simulation

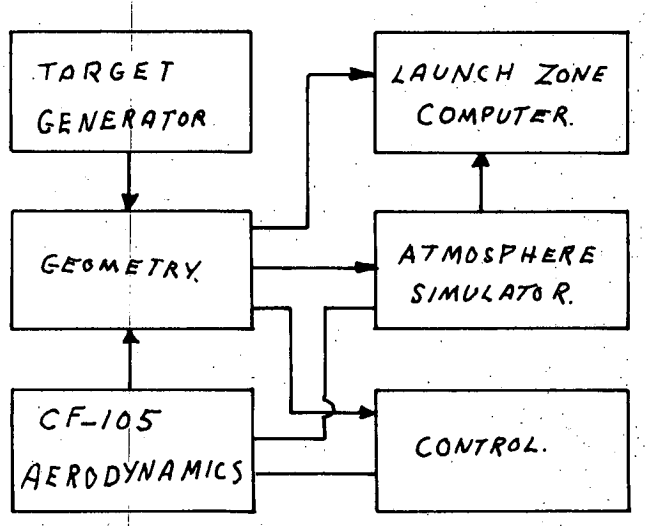

Figure 2 - Fire Control Geometry

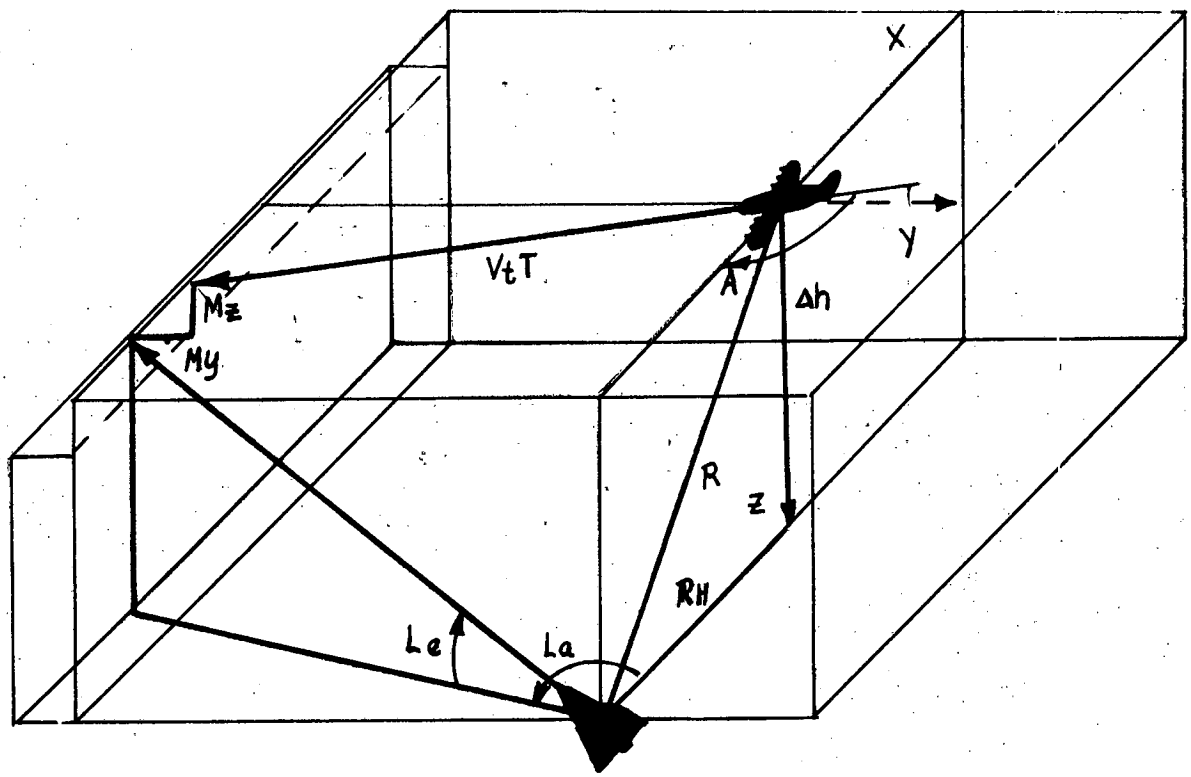

Figure 3 - The Navigation Law

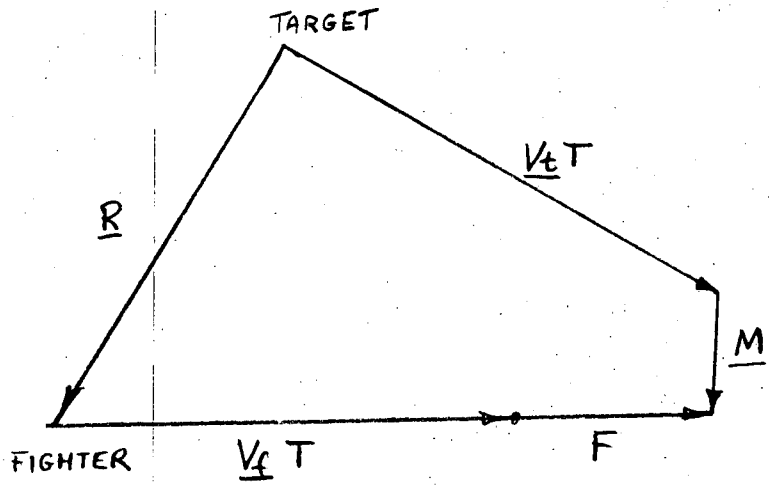

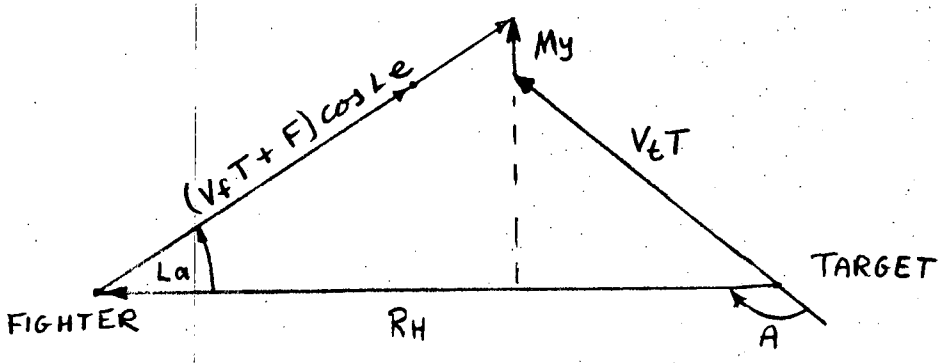

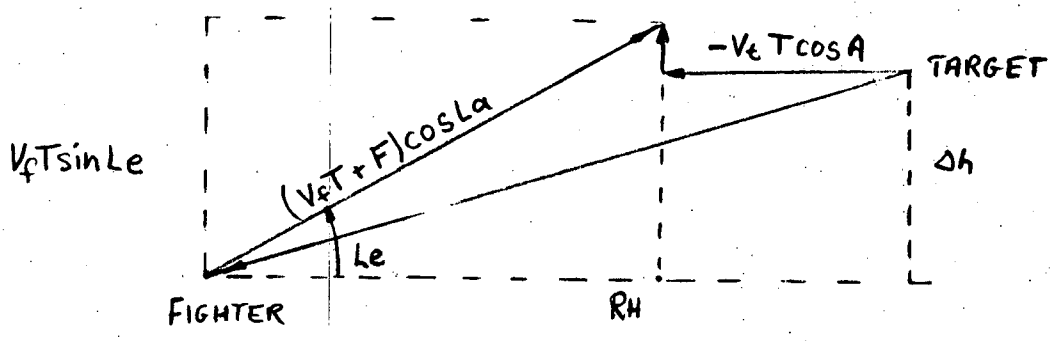

Figure 4 - Fighter Axes

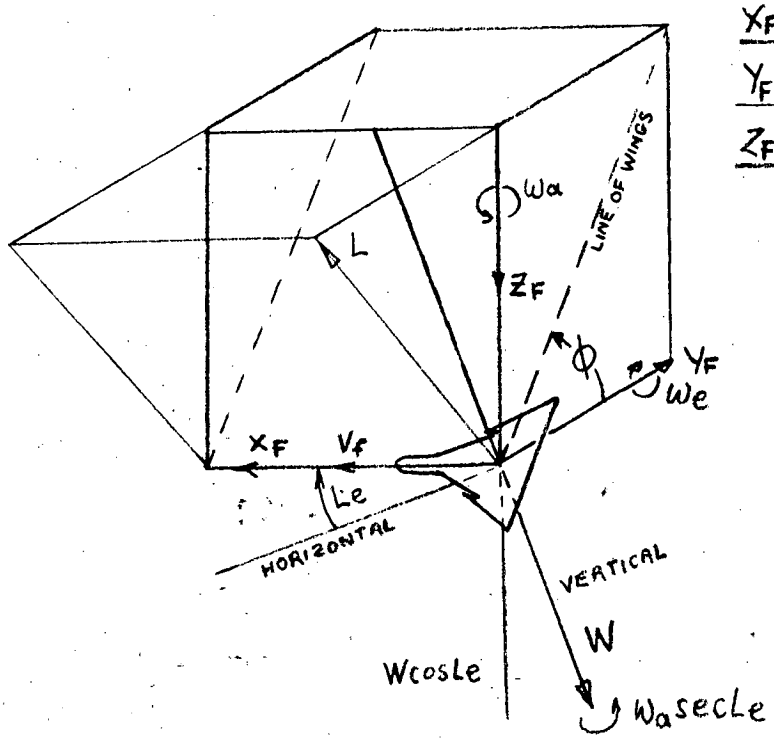

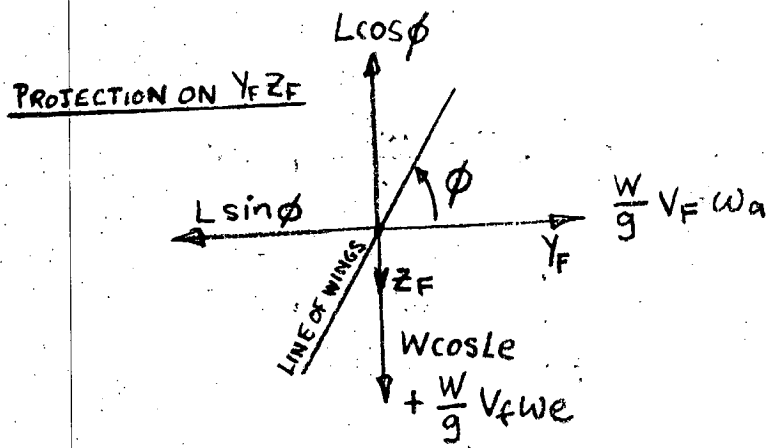

Figure 5 - A.I. Gimbal Deflections

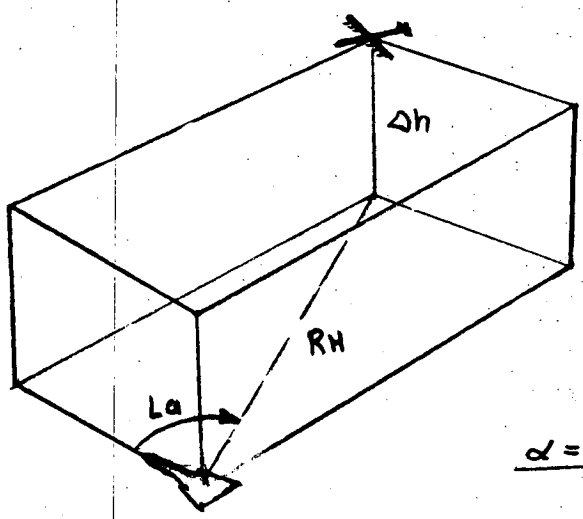

$\alpha = \phi = Le = 0$

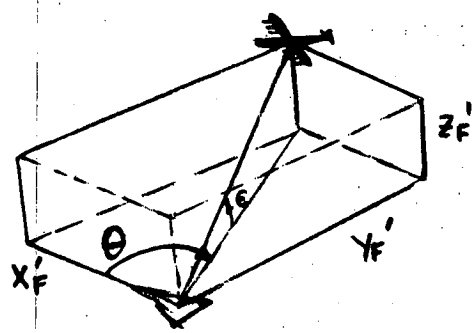

GENERAL CASE

Figure 6 - Thrust and Drag Carpet for CF-105

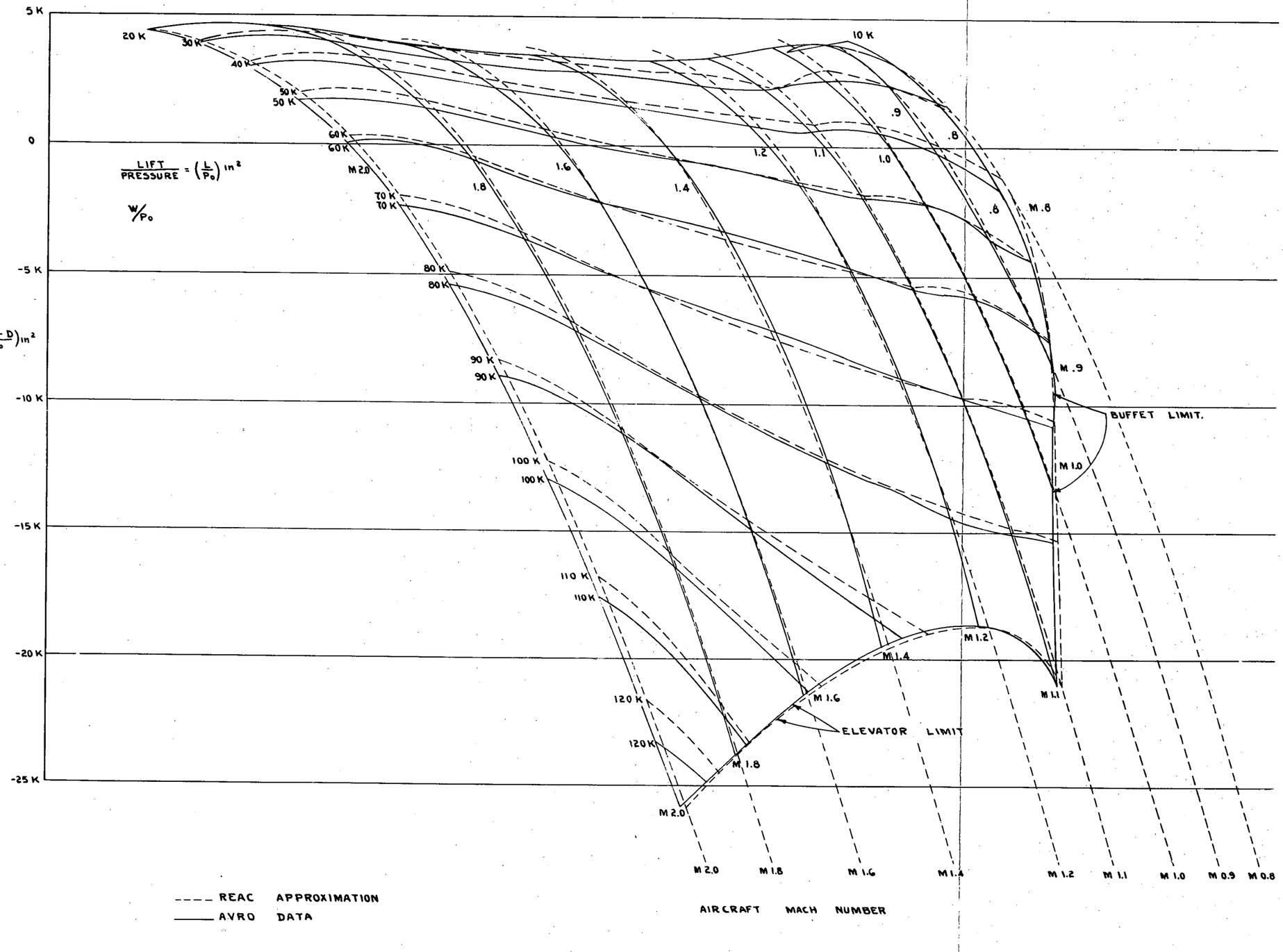

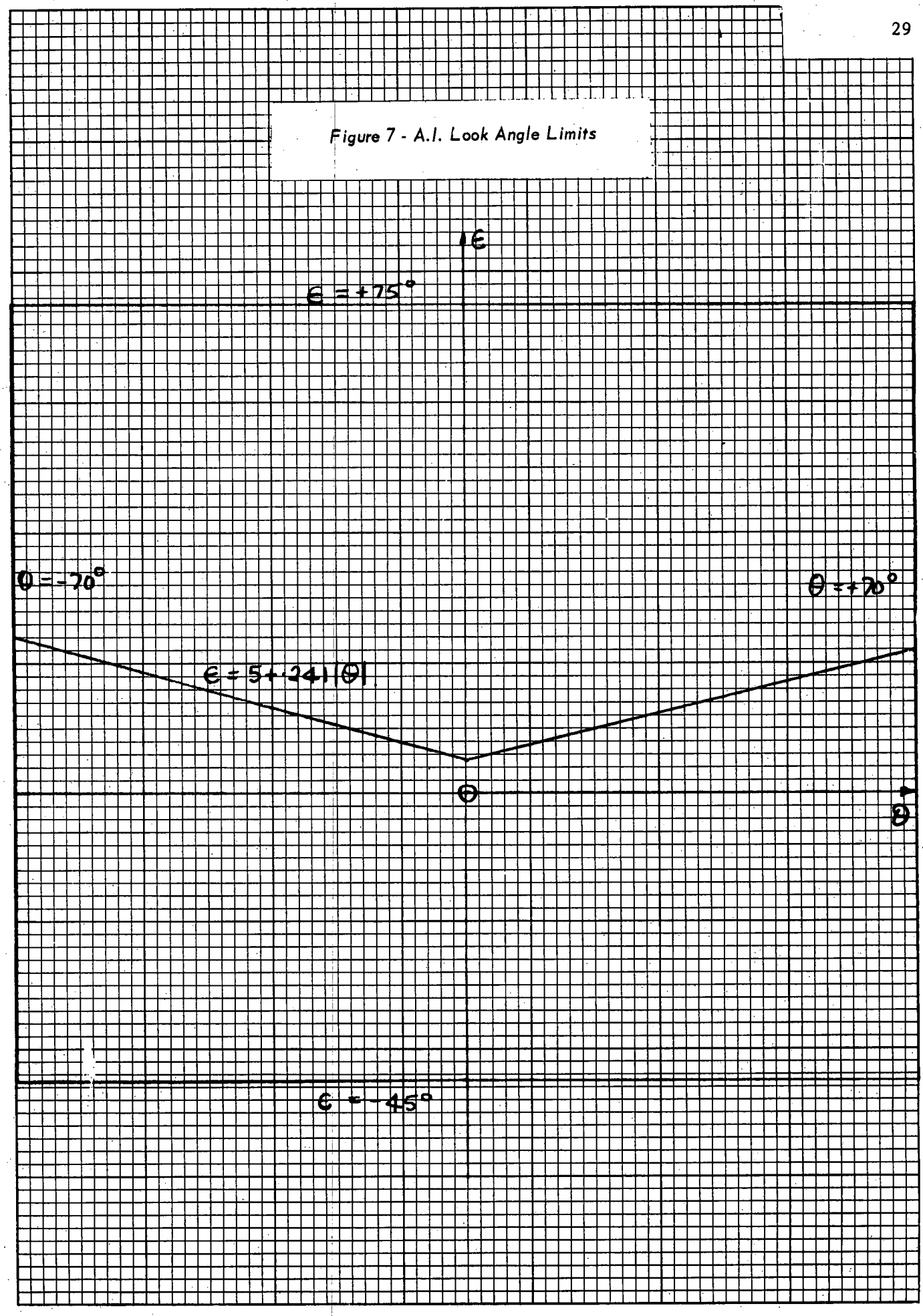

Figure 7 - A.I. Look Angle Limits

Figure 8 - Final Climb Angle for Various Initial Fighter Positions

Δh_0 = 20K INITIAL HEIGHT DIFFERENCE

h_{f_0} = 40K INITIAL FIGHTER HEIGHT

F pole = 7K

MISSILE FLIGHT TIME 8 SEC.

$M_{f_0} = M_t = 2.0$

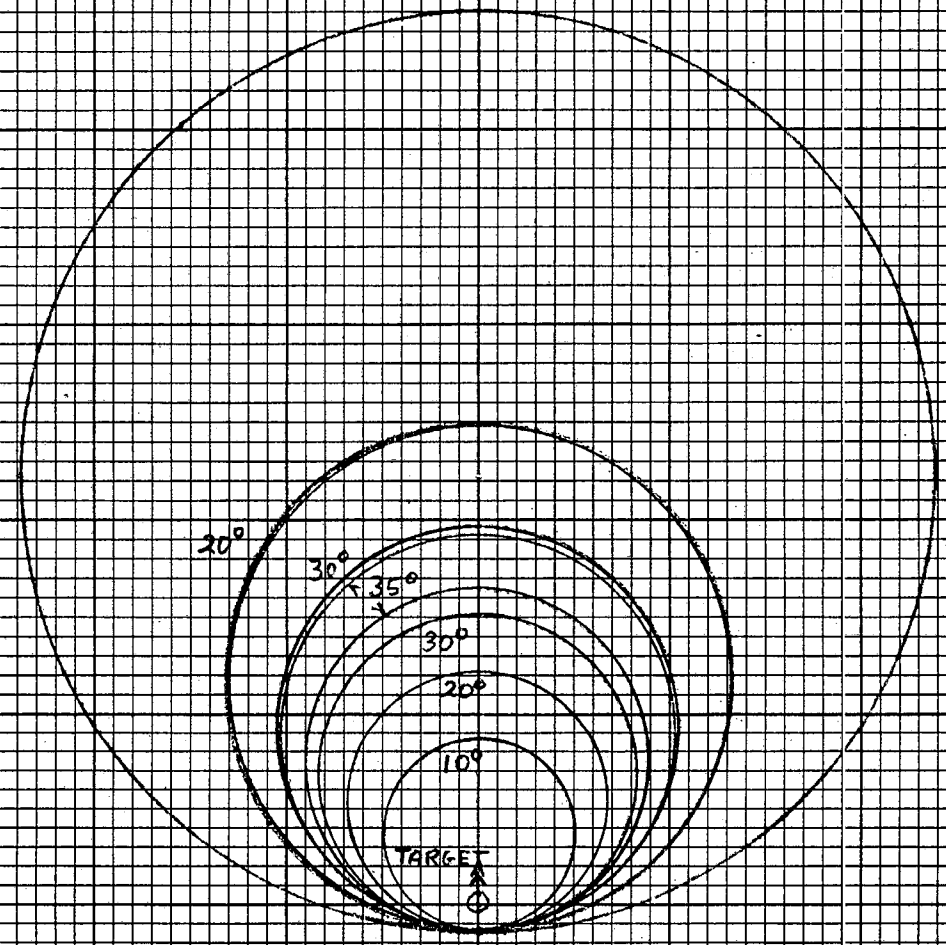

SCALE 50,000 ft/inch

Figure 9 - Errors in Closing Rate and Climbing Rate

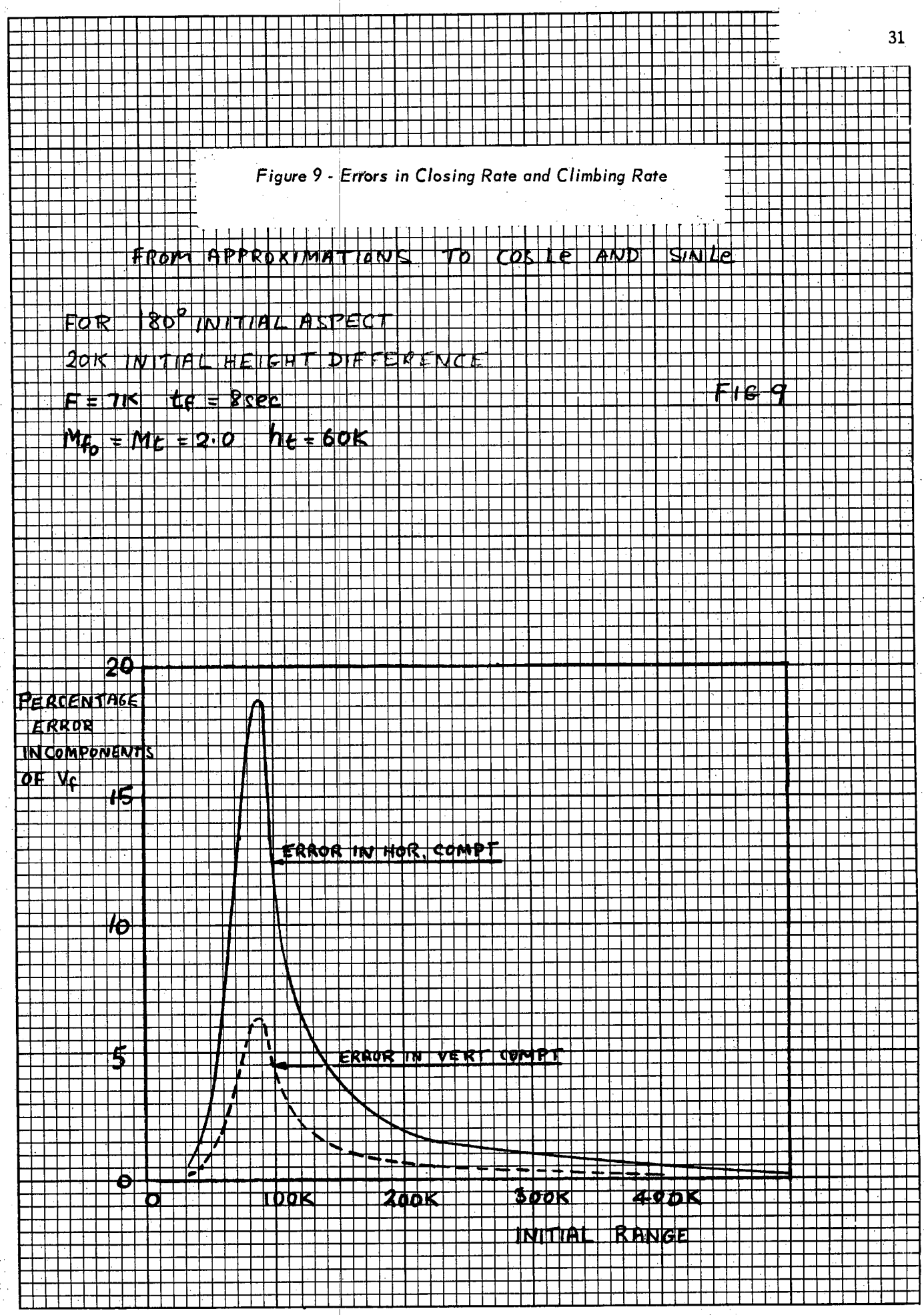

Figure 10 - Errors in Components of Fighter Velocity

ERROR IS DUE TO GEOMETRIC APPROXIMATIONS

$M_{f_0} = 2.0$

$M_E = 2.0$

$\Delta h_0 = 20K$

$\theta_{sec} = 4°$

$F = 7K$

PERCENTAGE ERROR IN COMPONENTS OF FIGHTER VELOCITY

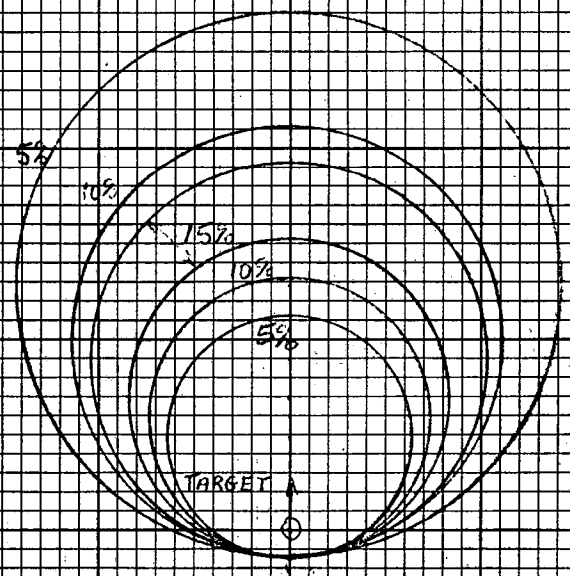

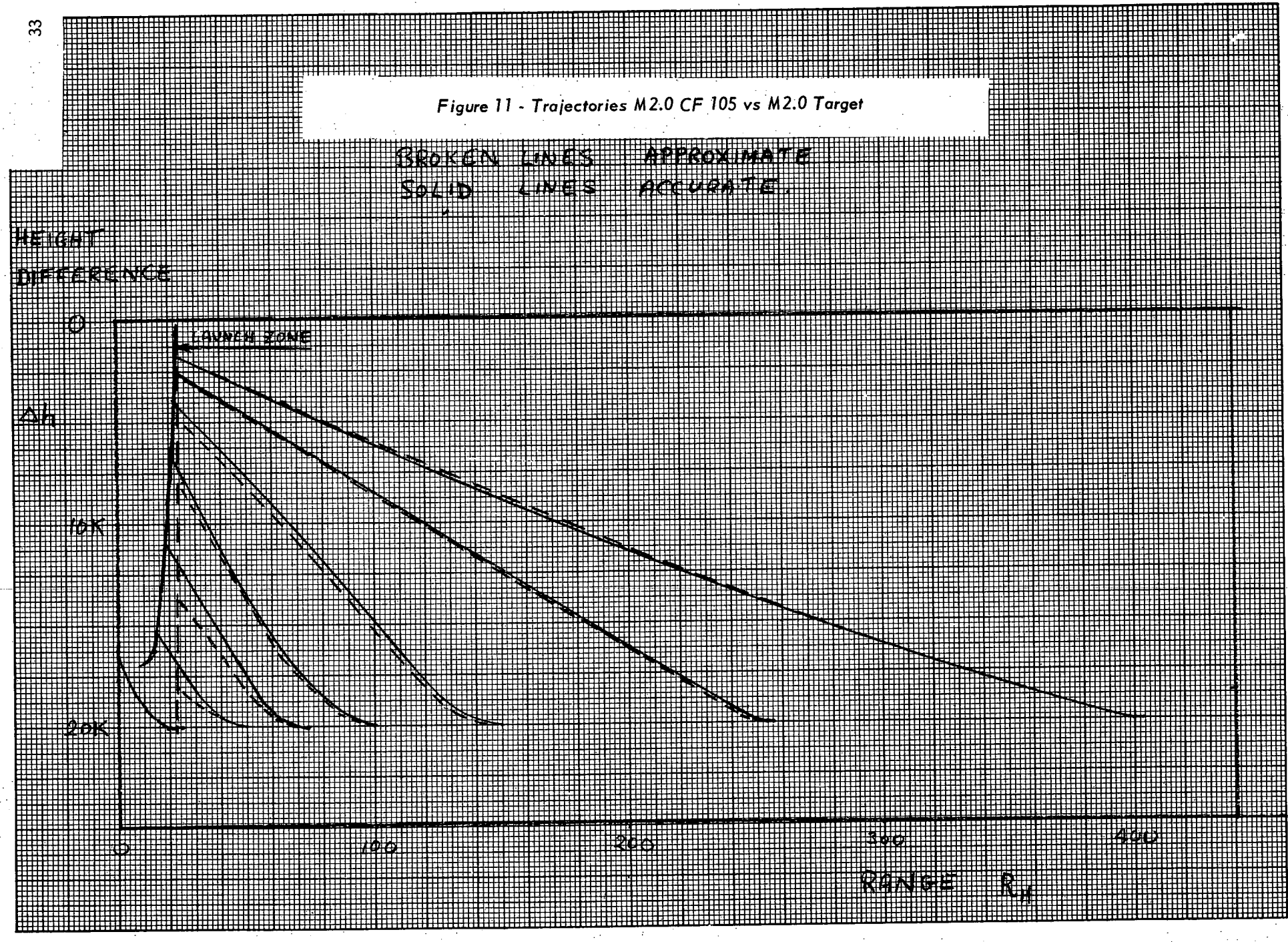

Figure 11 - Trajectories M2.0 CF 105 vs M2.0 Target

Figure 12 - Results of Trigonometry Approximation Study

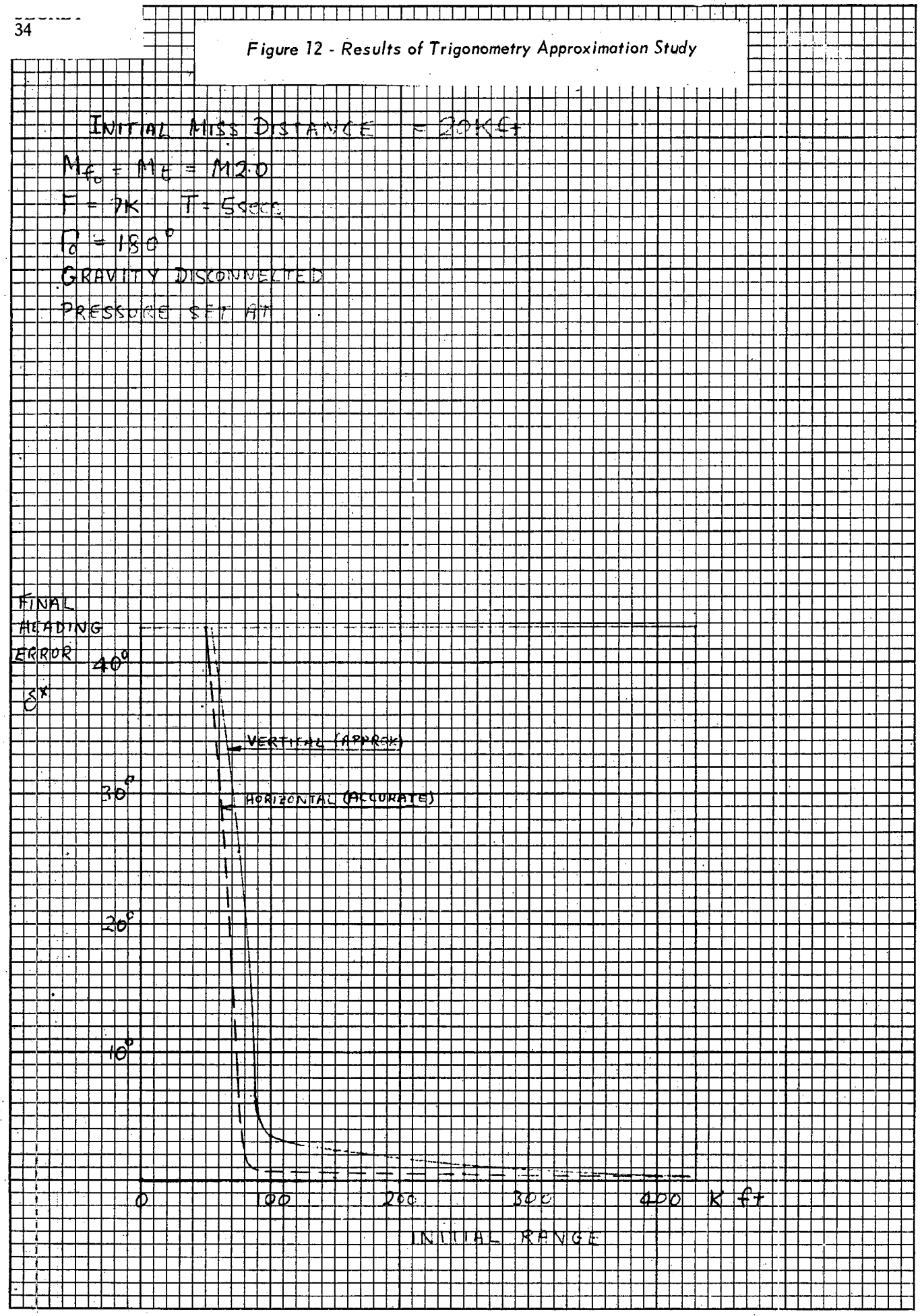

Figure 13 - Final Climb Angle vs Initial Range

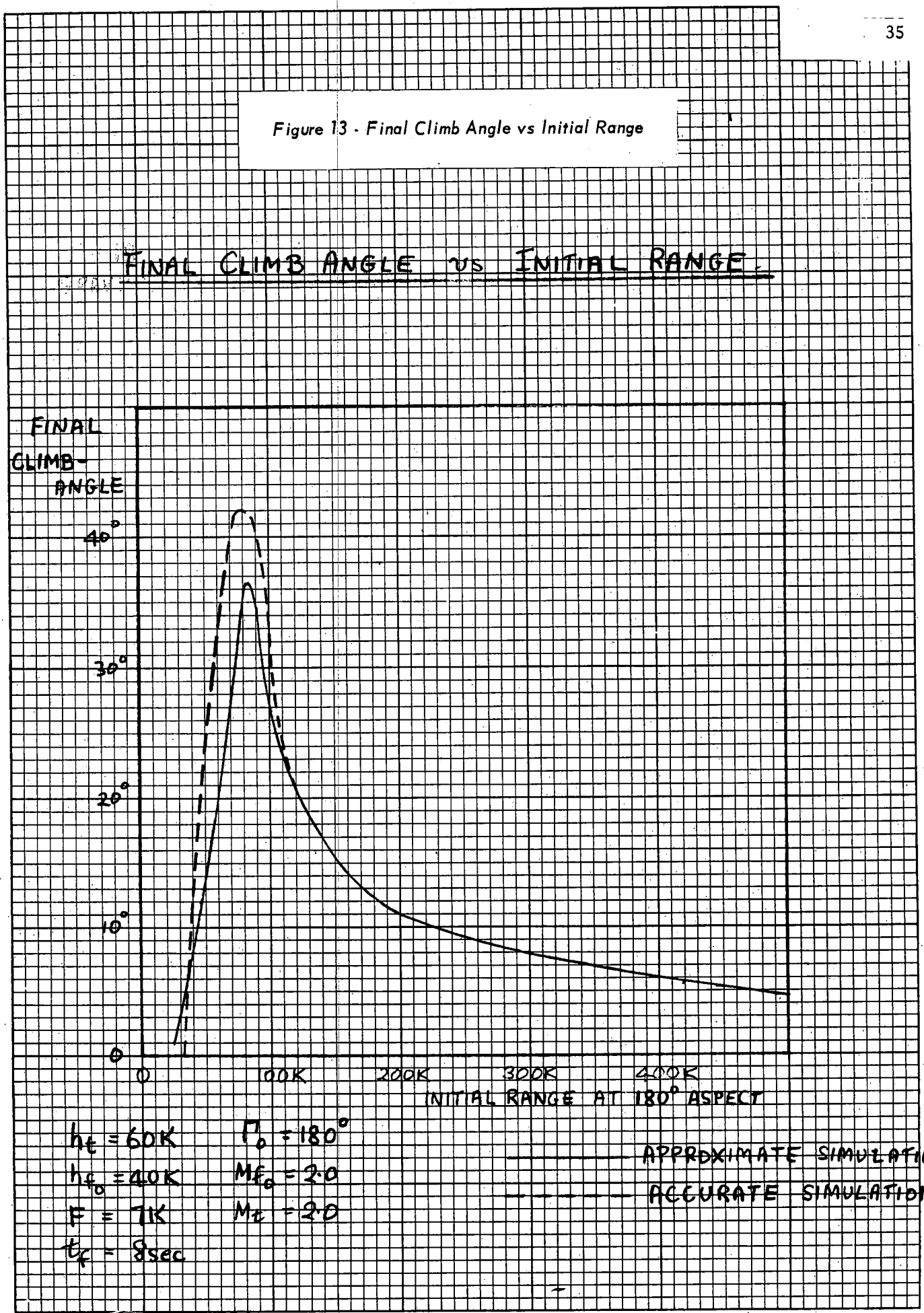

Figure 14 - Error in Location of Fall-Back and Minimum Velocity Placement Barriers

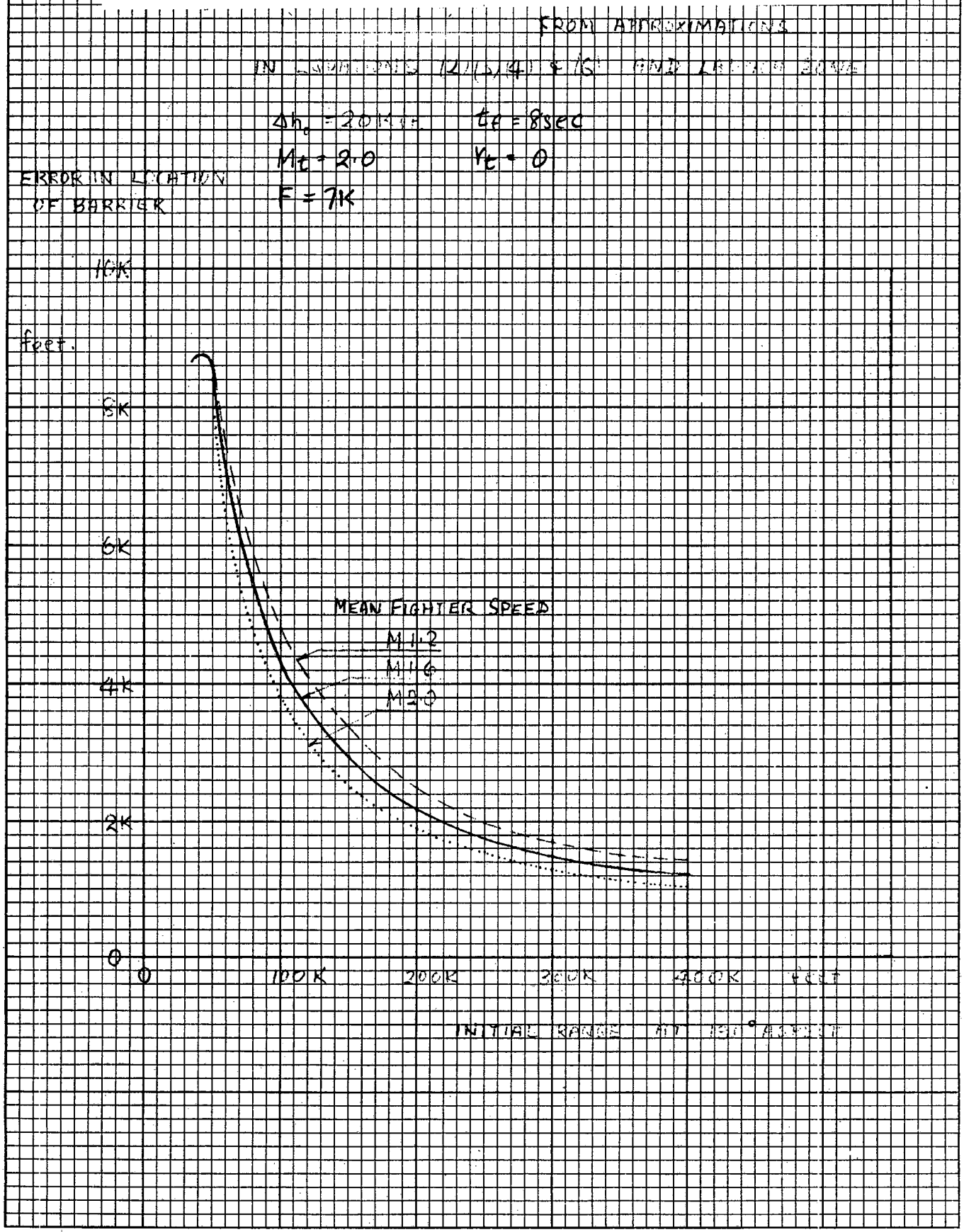

Figure 15 - Error in Location of Fall-Back and Minimum Velocity Barriers

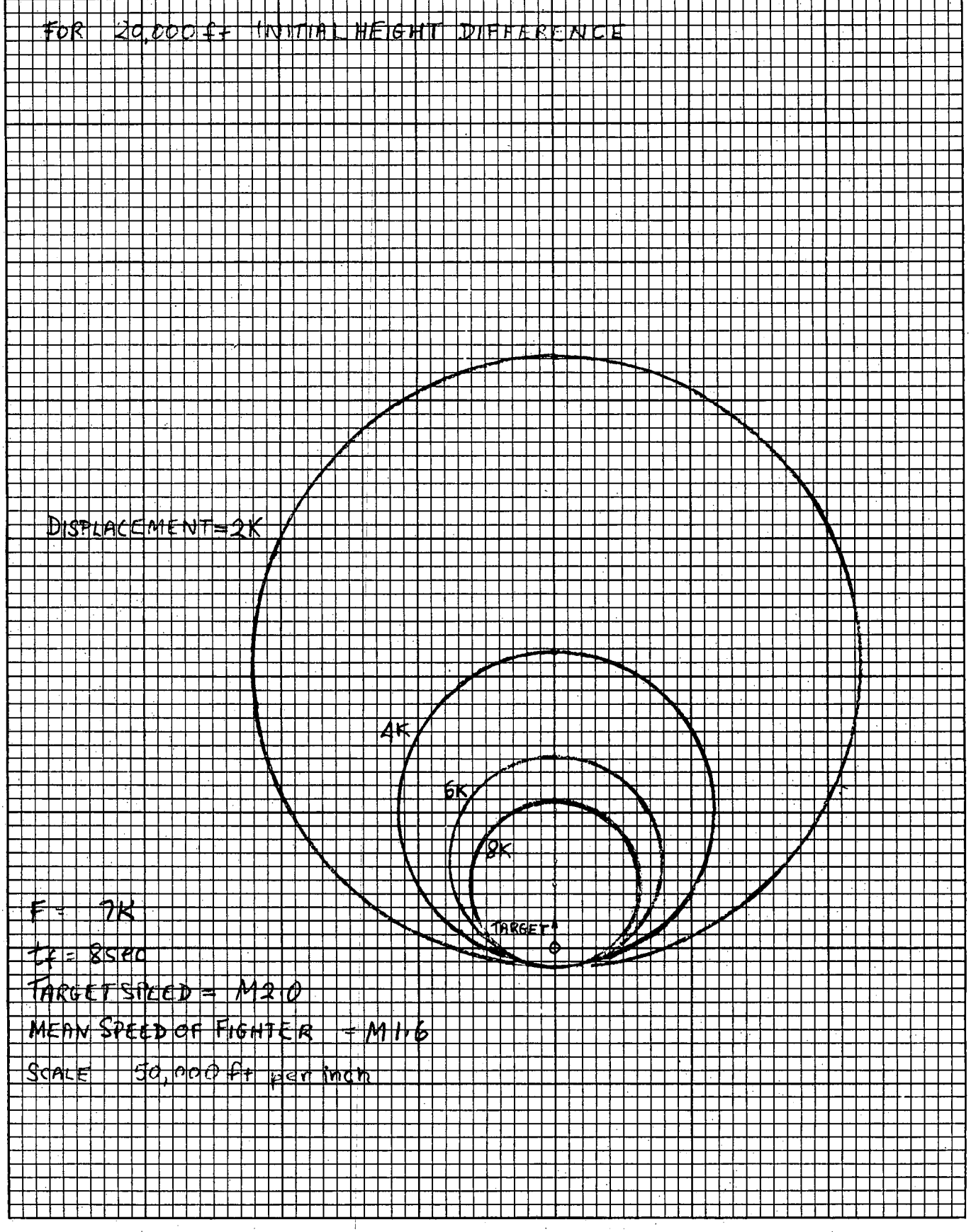

Figure 16 - Displacement of Look Angle-Barriers by $\frac{Mz}{T}$ and $\frac{Mr}{T}$ Limits

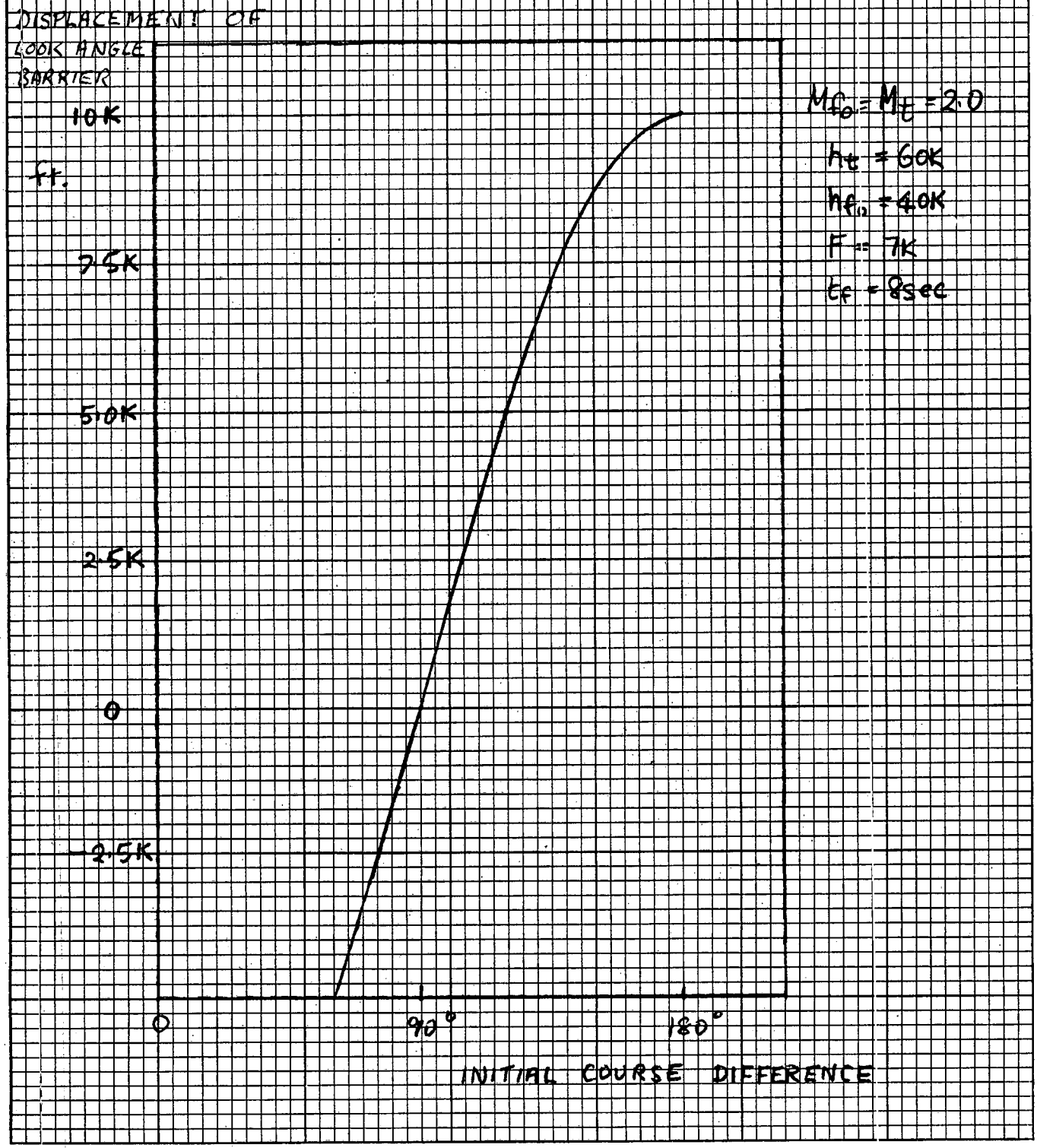

Figure 17 - Accuracy of Heading Error Calculation

REAC CALCULATES $\delta^x = \sqrt{(La-La^x)^2+(Le-Le^x)^2}$

ACCURATELY $\cos\delta^x = \cos La \cos La^* (\cos\{La-La^*\}) + \sin La \sin La^*$

The difference is shown below as a fraction of δ^x REAC.

The calculations have been done for $\delta^x = 25°$ and $\delta^x = 15°$

δ^x = heading error at launch.

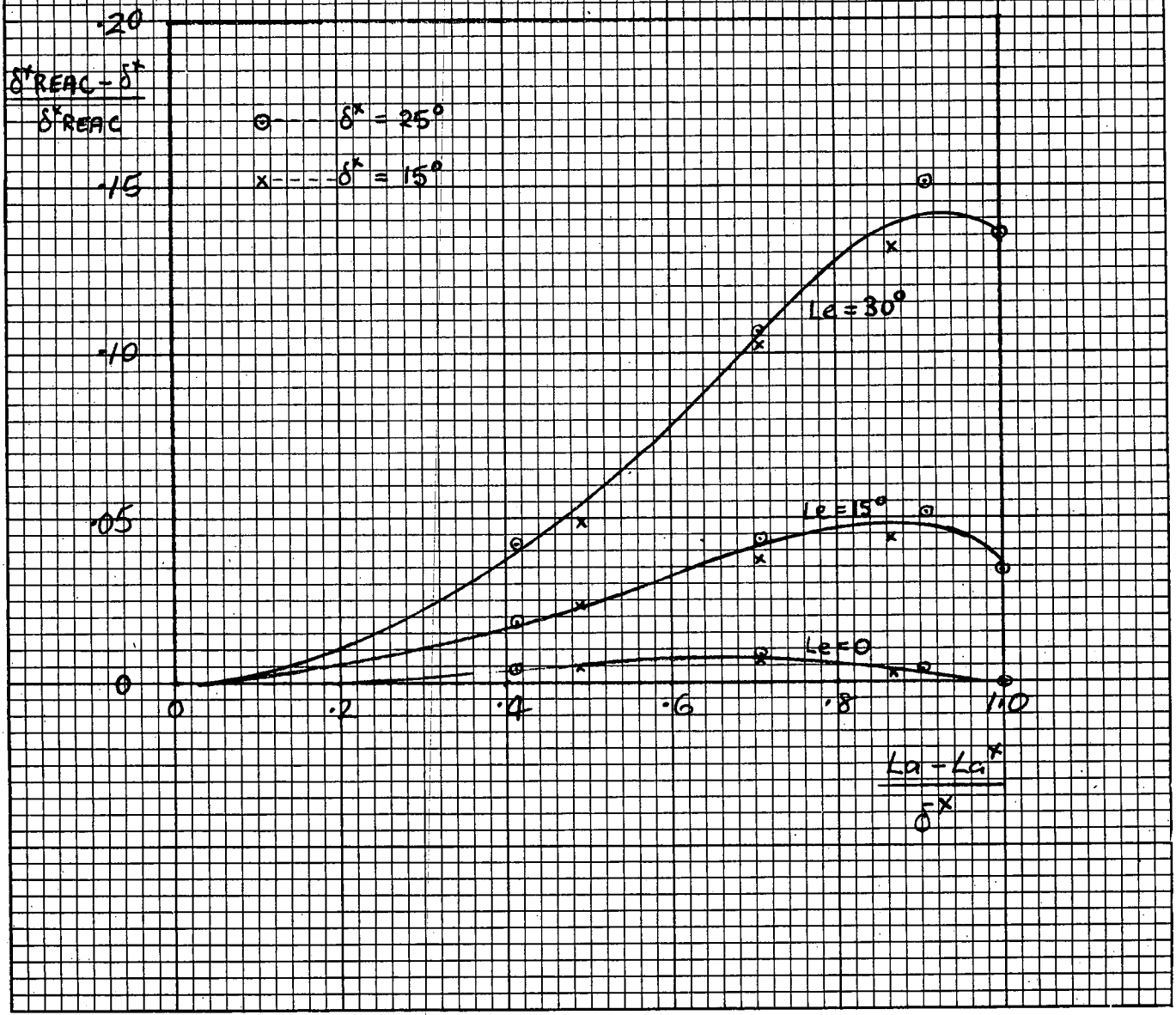

Figure 18 - Launch Zones t_f = Constant

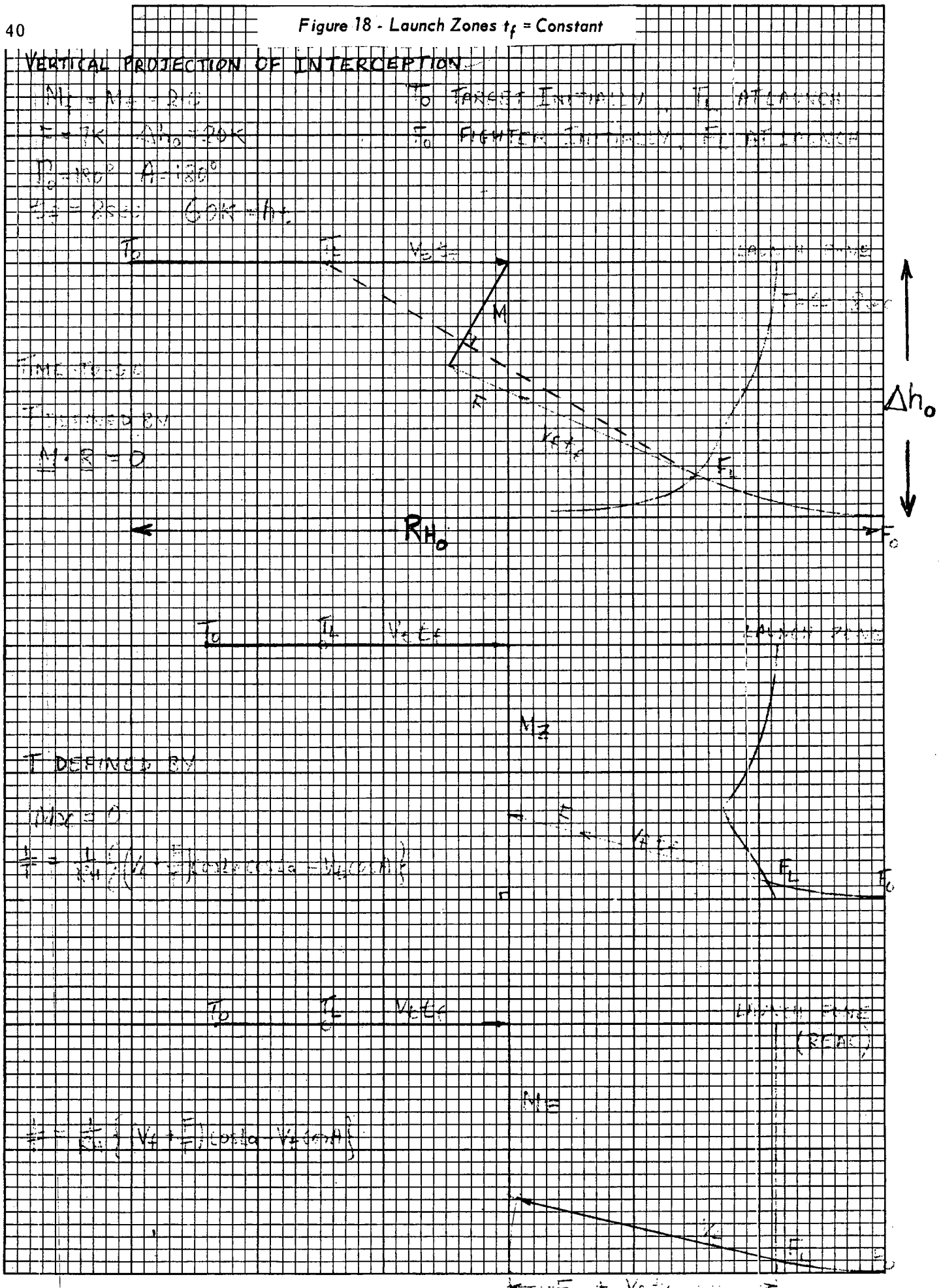

Figure 19 - Effect of Geometric Approximations Shift of Maneuver Barrier

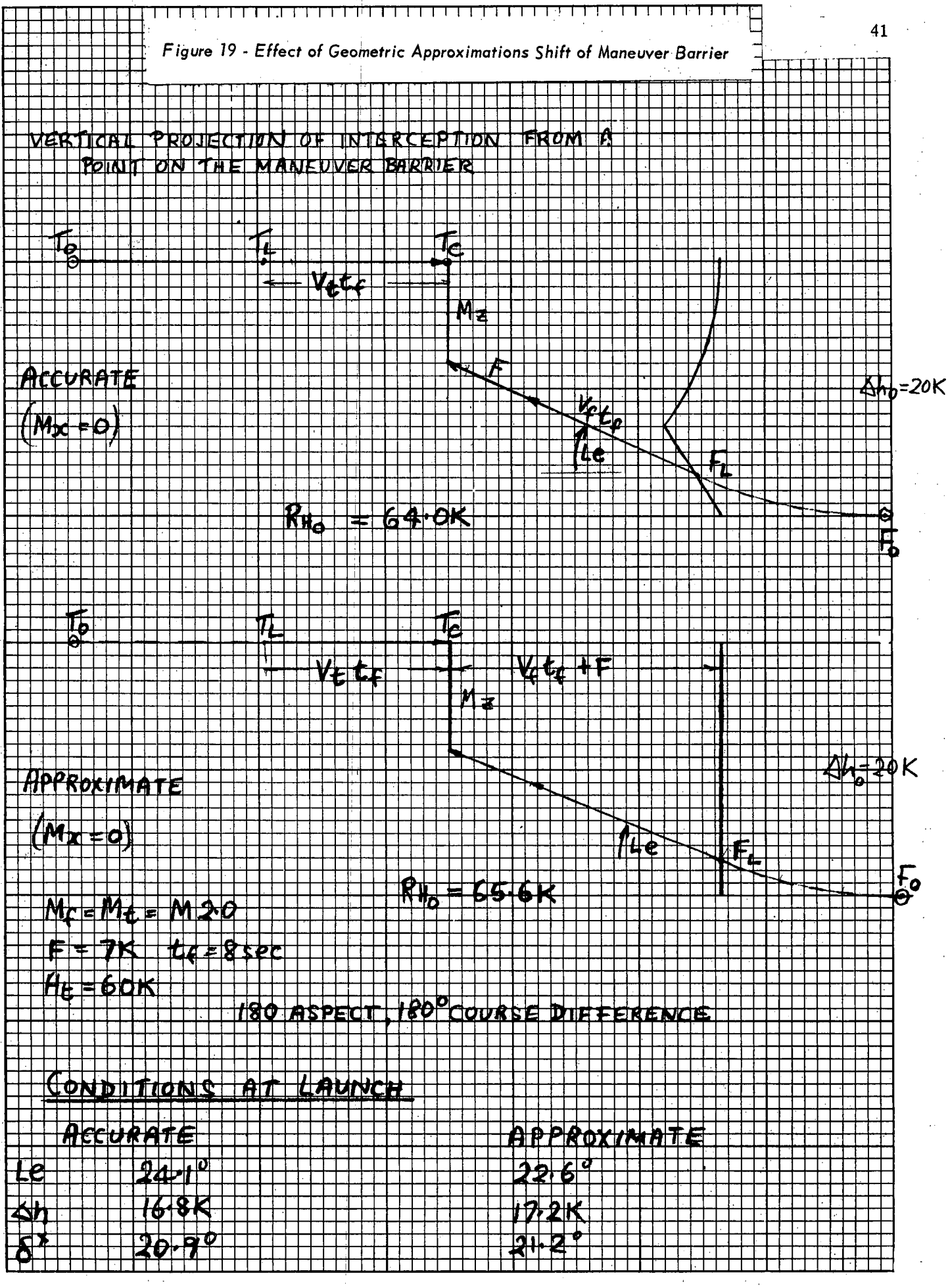

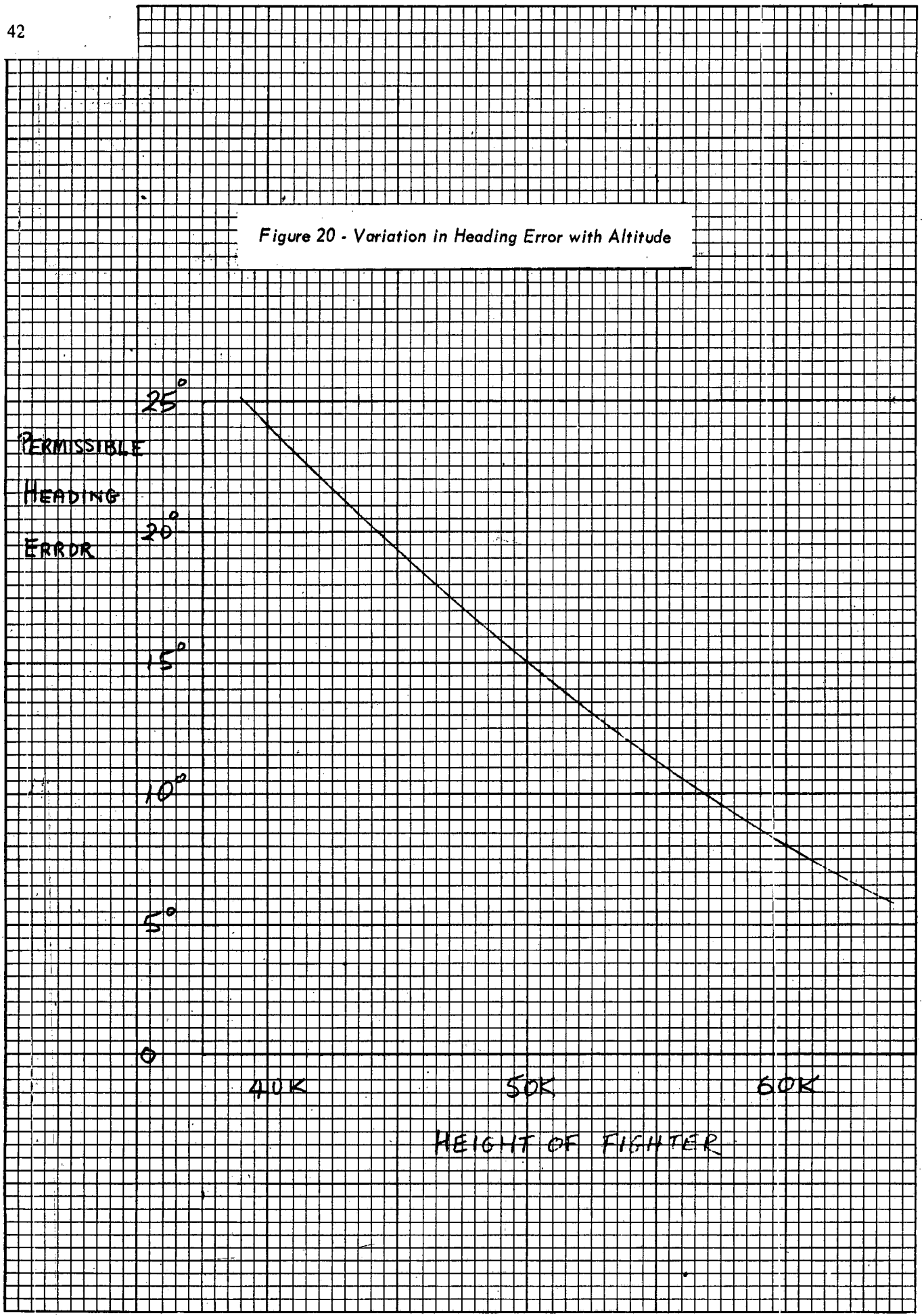

Figure 20 - Variation in Heading Error with Altitude

Figure 21 - Derivation of Angle of Attack

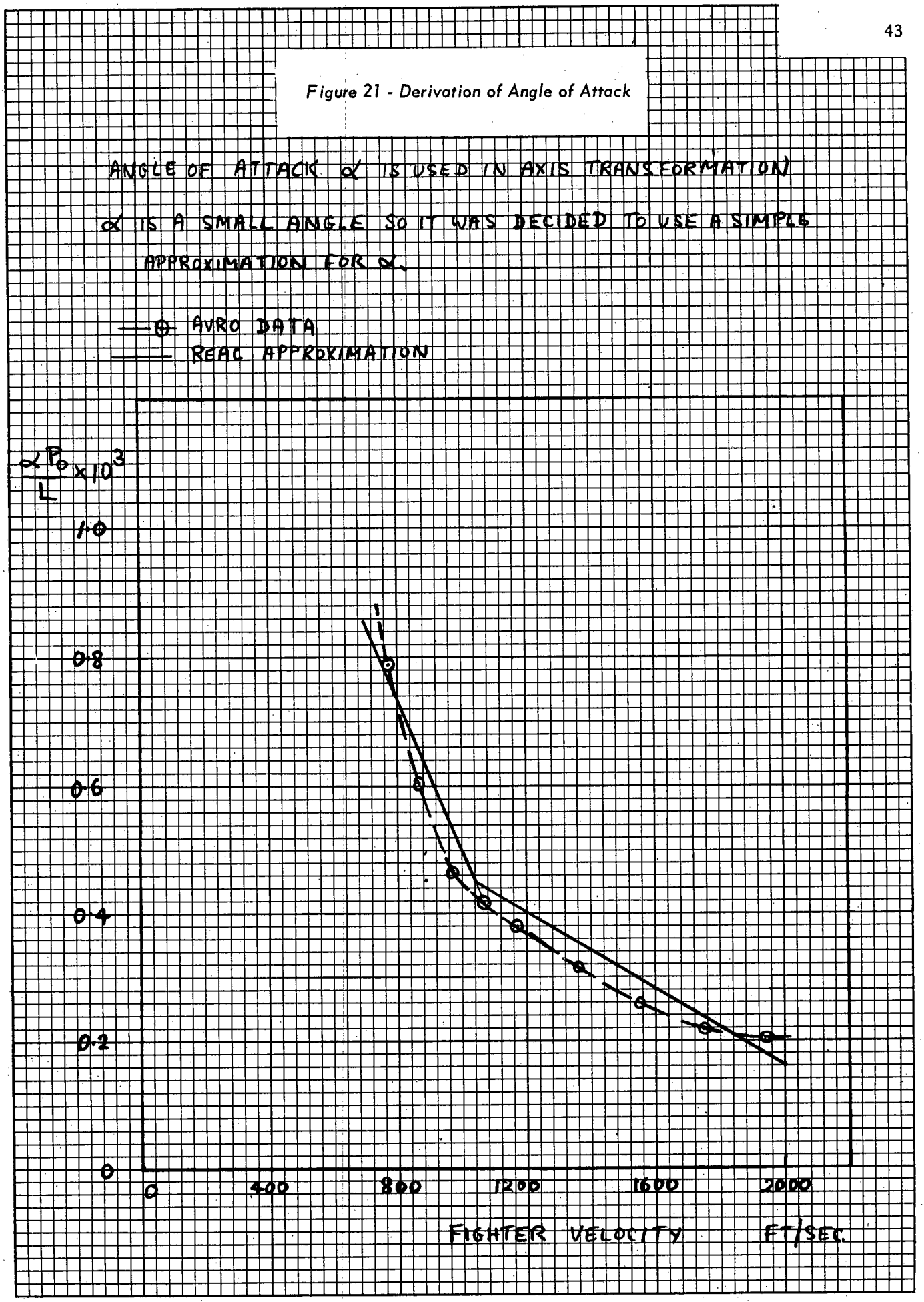

Figure 22 - Rotation of Look Angle Barrier About Offset Point

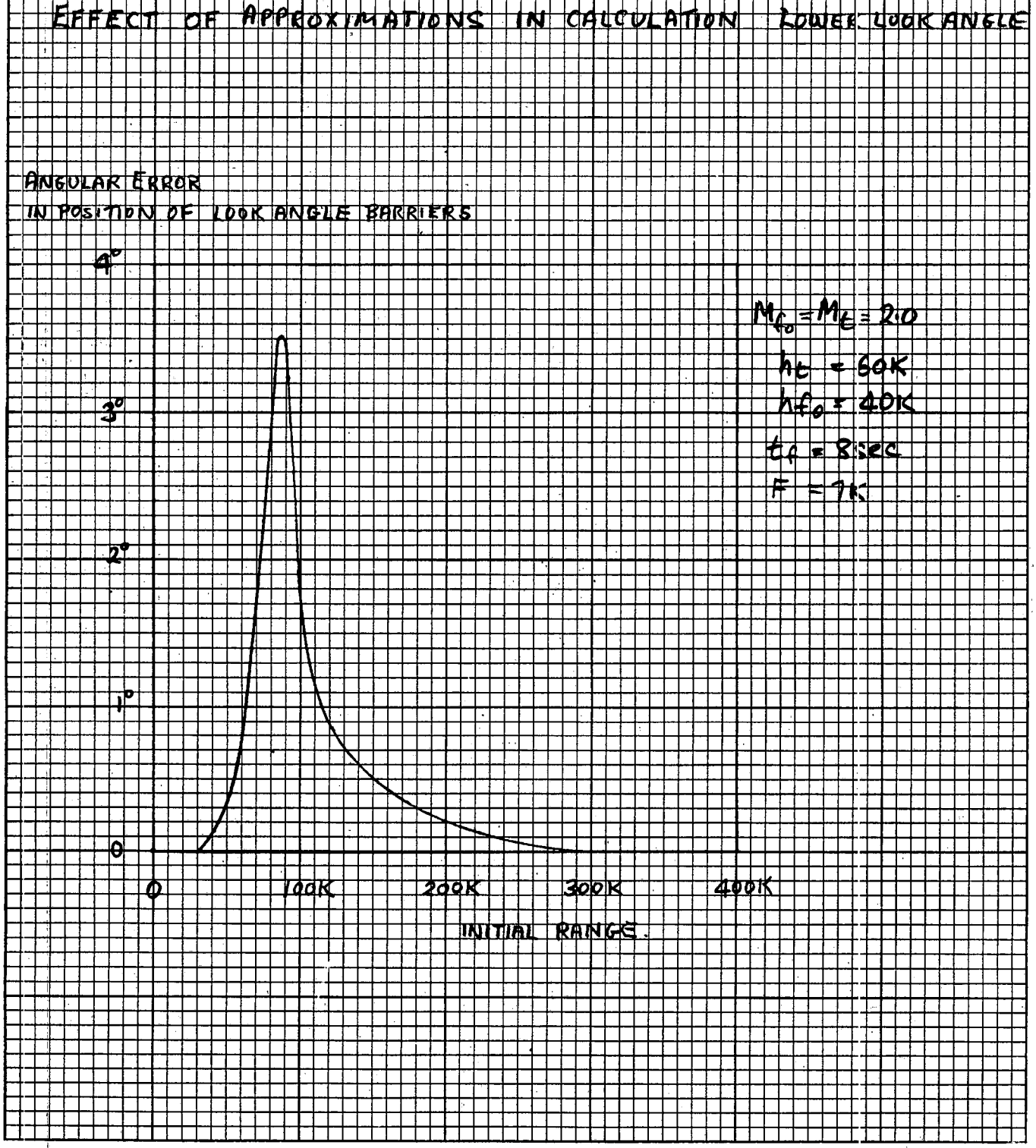

Figure 23 - Displacement of Look-Angle Barriers

FROM APPROXIMATIONS IN CALCULATION OF ϵ

THE DISPLACEMENT IS MEASURED NORMAL TO THE LINE JOINING THE INITIAL FIGHTER POSITION AND THE OFFSET POINT AND IS CLOCKWISE IN THE RIGHT HALF PLANE

$h_{f_0} = 40K \quad M_{f_0} = M2.0$

$h_t = 60K \quad M_t = M2.0$

$F = 7K$

$t_f = 8sec$

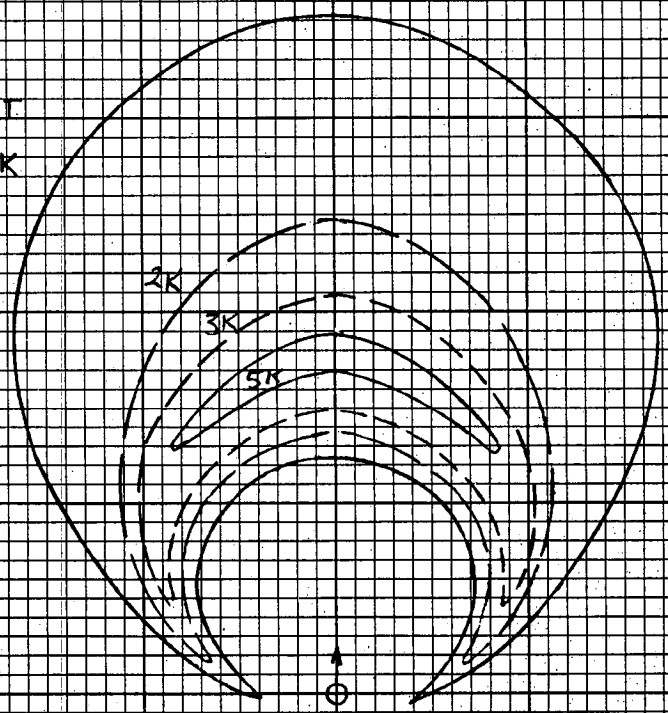

SCALE 50,000 ft/in.

Figure 24 - Effect of Steering Control Gain

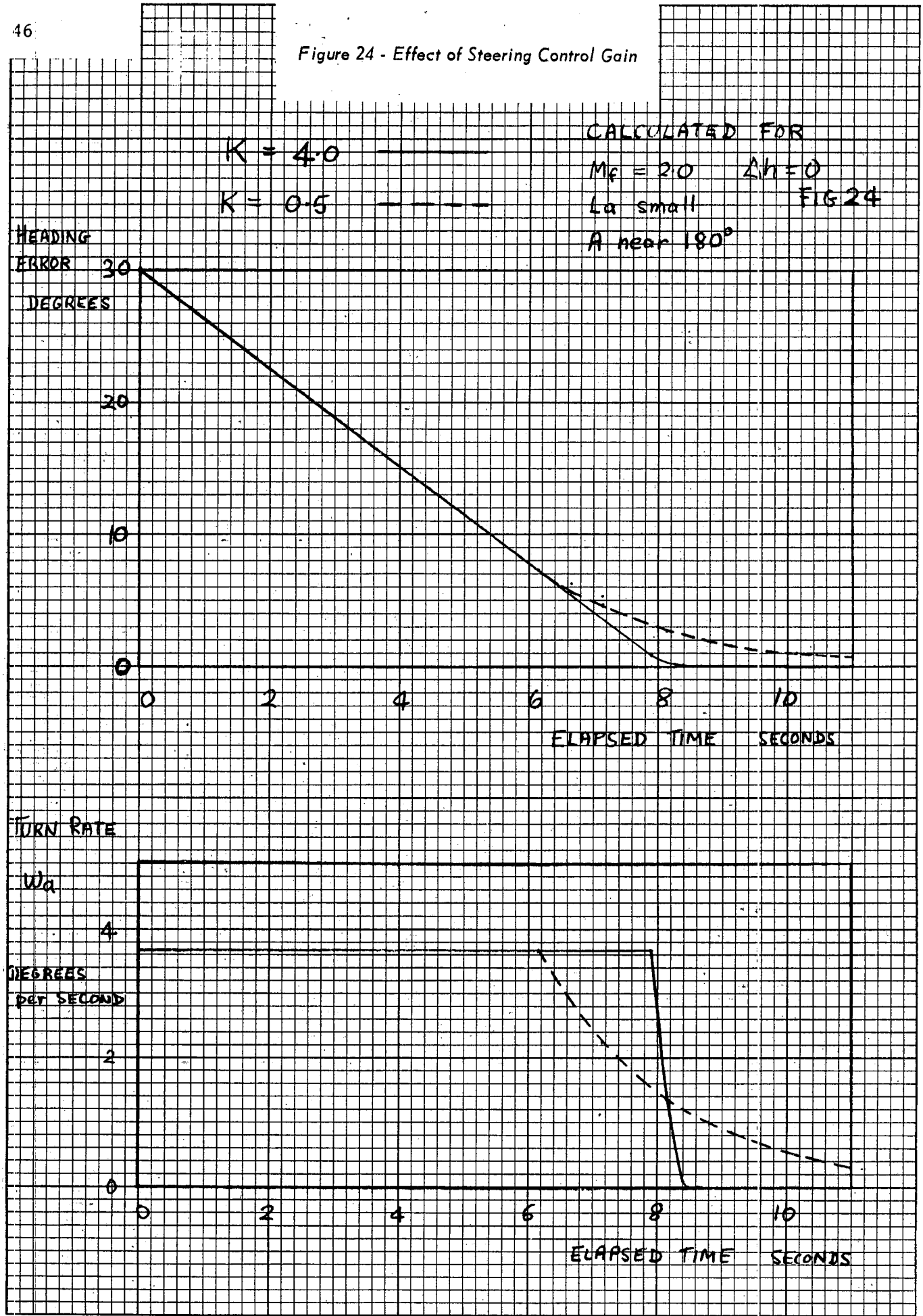

Figure 25 - Effect of Change in Time-to-Go at Snap-Up

$\Gamma_o = 110°$

$M_{f_o} = M_t = 2.0$ $H_t = 60K$

$t_f = 8sec$ $F = 7K$ $H_{f_o} = 40K$

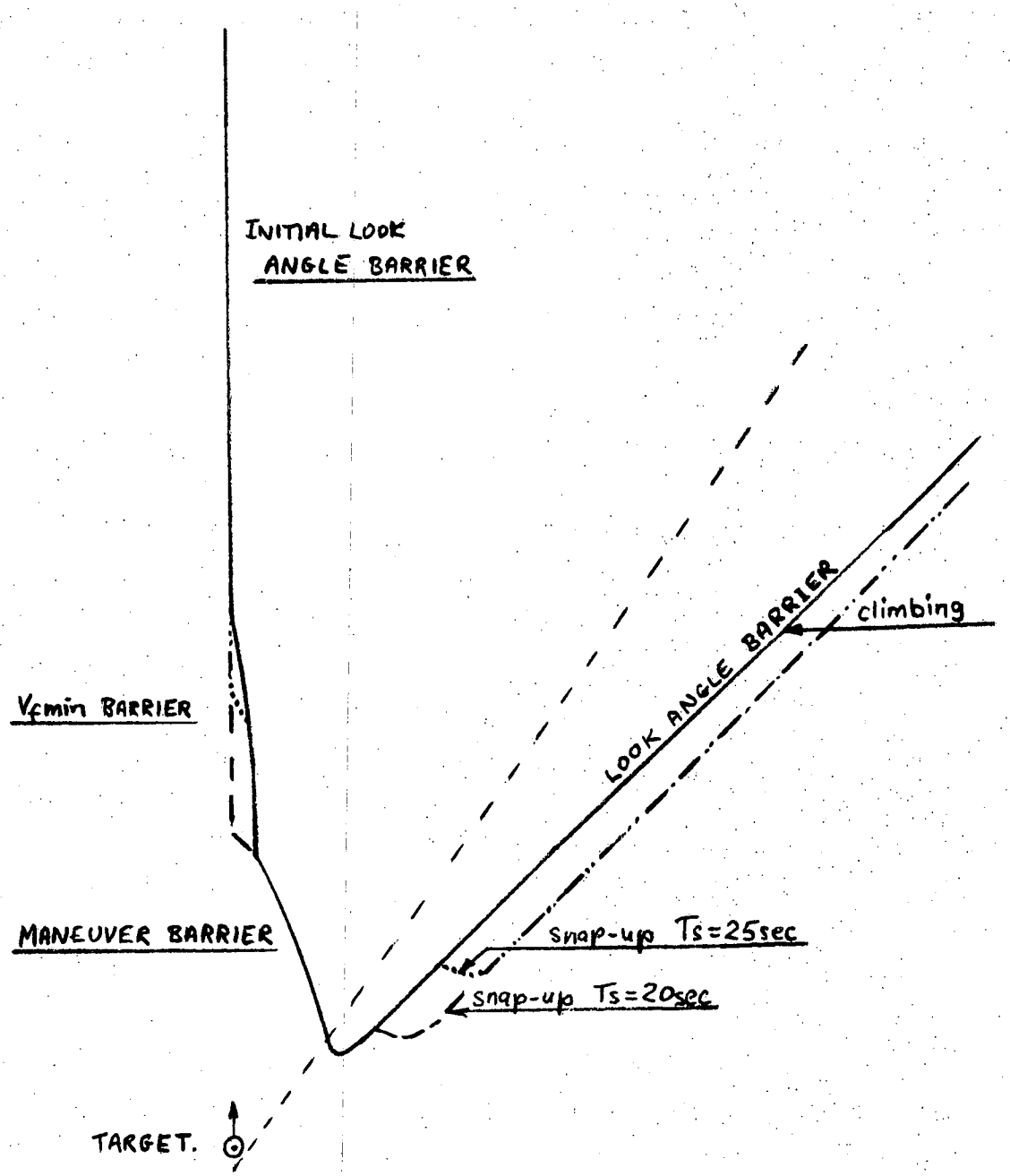

Figure 26 - Effect on Placement Zone of Some REAC Approximations

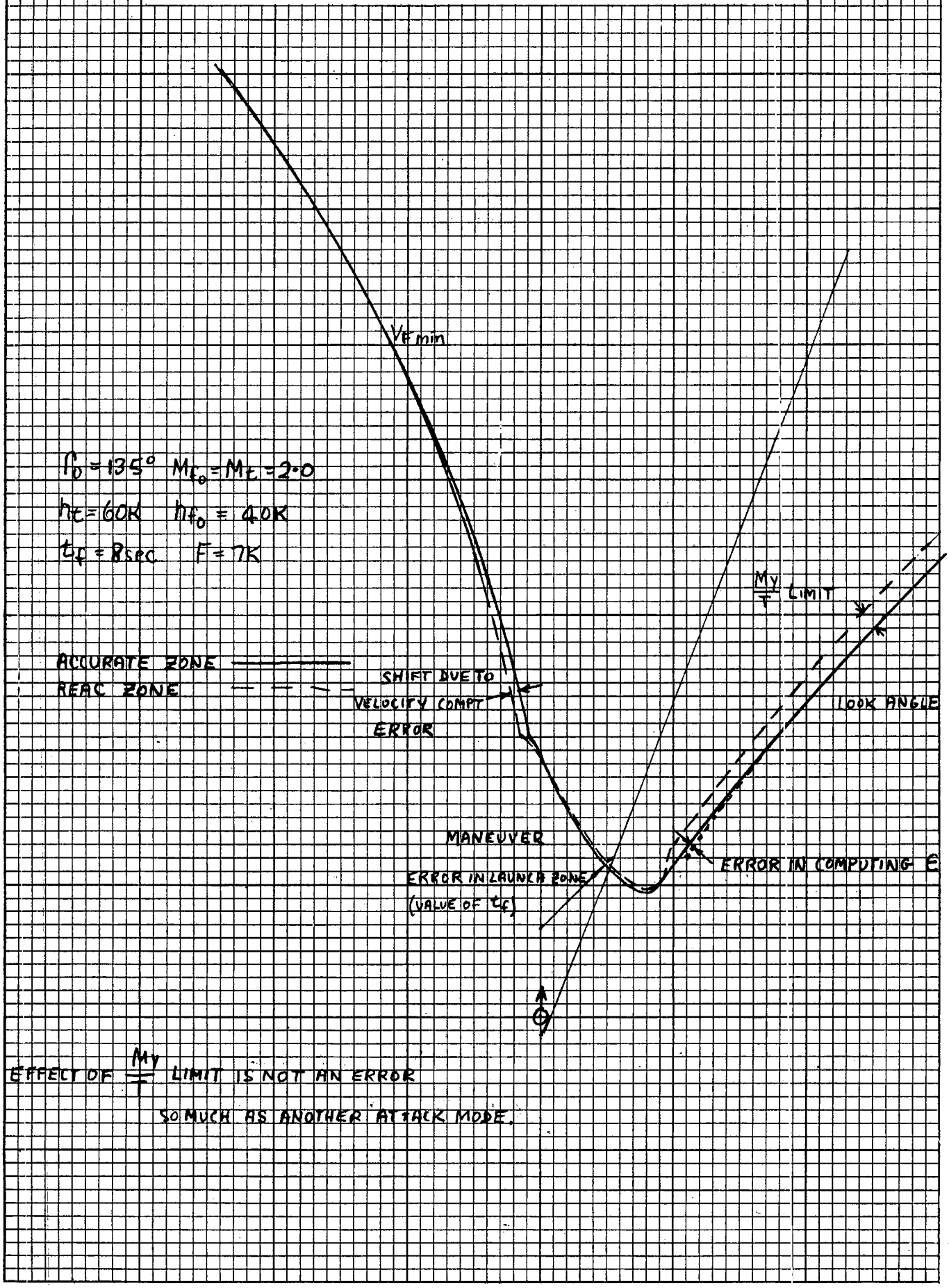

Figure 27 - Effect of REAC Approximations

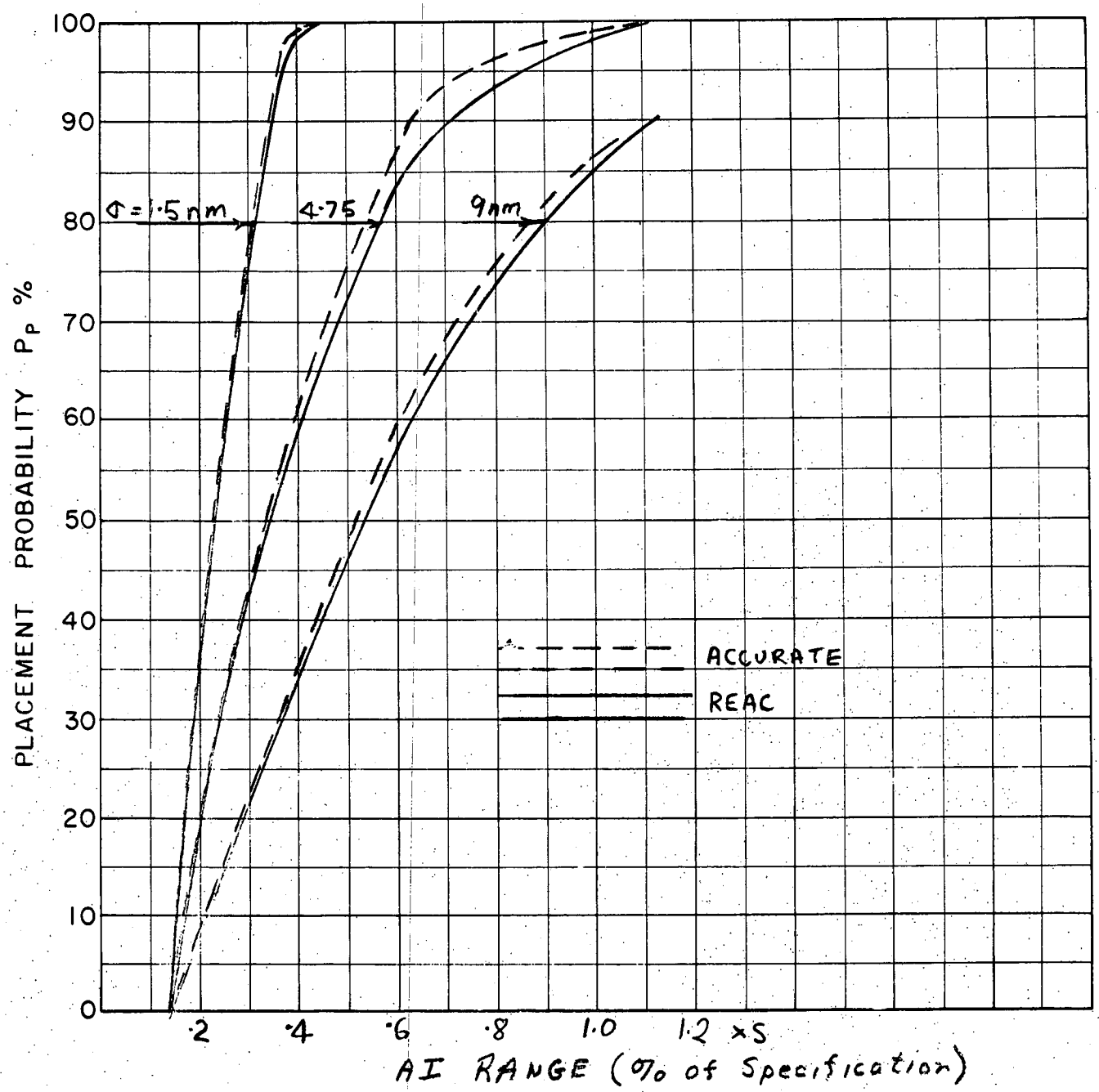

COURSE DIFFERENCE: 135°
TARGET EVASION: 0
TARGET MACH NO.: 2.0
INTERCEPTOR LATERAL G's: AVRO 3·3
INTERCEPTOR MACH NO.: 2.0
σ OF G.C.I. ACCURACY: 1.5, 4.75, 9 nm.
A.I. DETECTION RANGE AS FRACTION OF SPECIFICATION RANGE, S: Abscissa
A.I. DETECTION RANGE CONTOUR: DELTA
ALTITUDE: H_{f_0} = 40K
H_t = 60K

Figure 28 - R_H, Δh, F/T, and 1/T Circuits

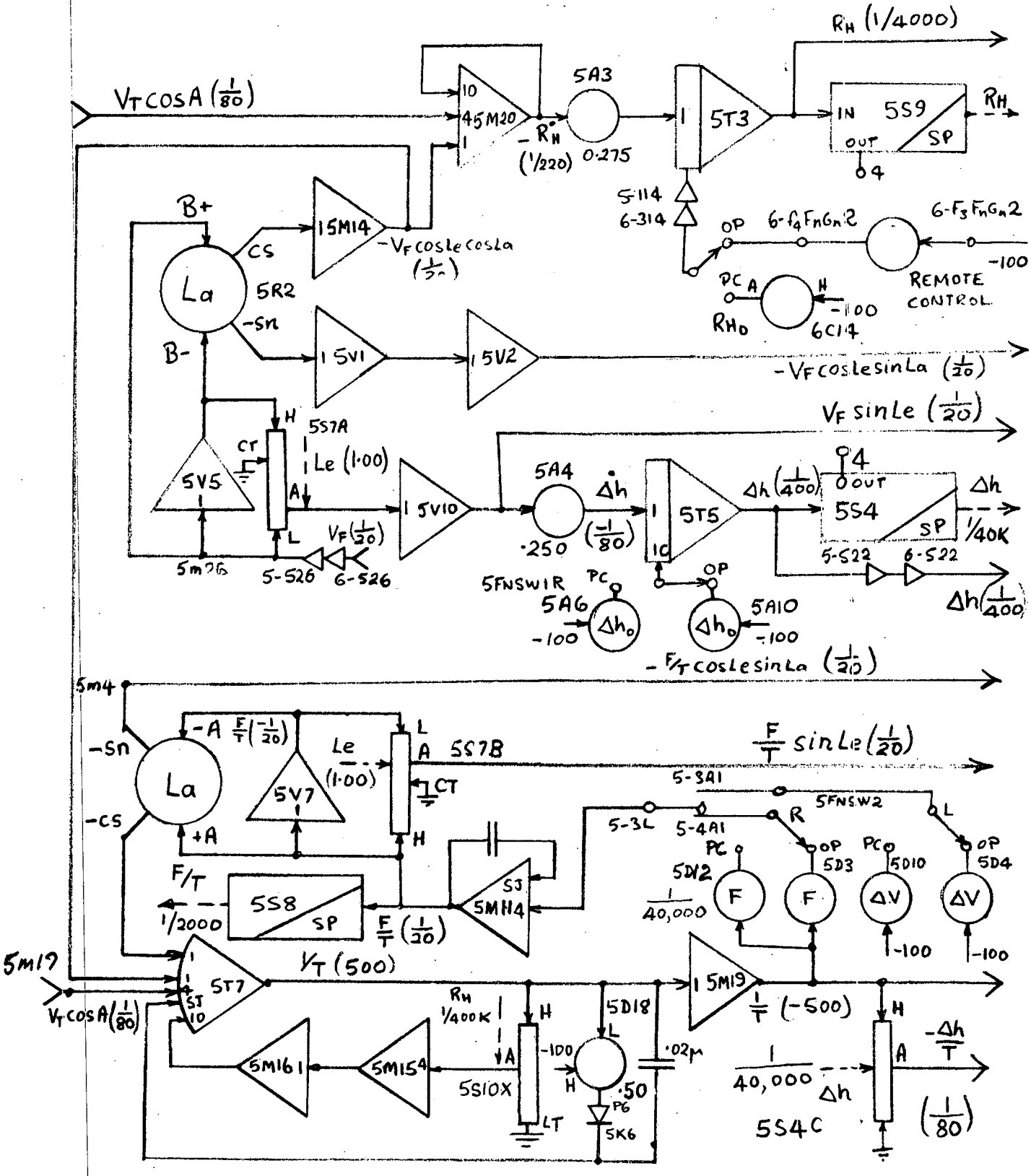

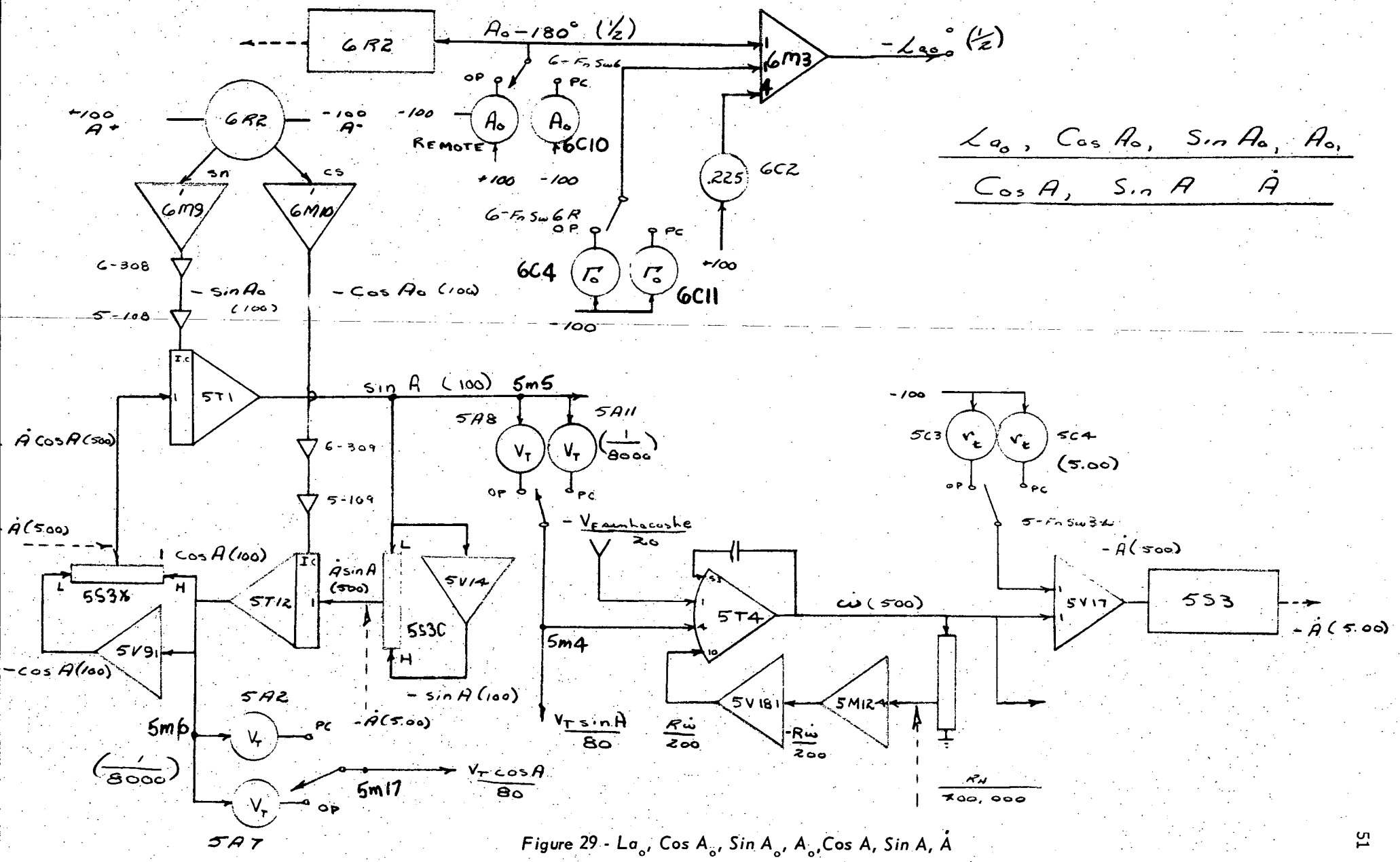

Figure 29 - La_o, Cos A_o, Sin A_o, A_o, Cos A, Sin A, $\dot{A}$

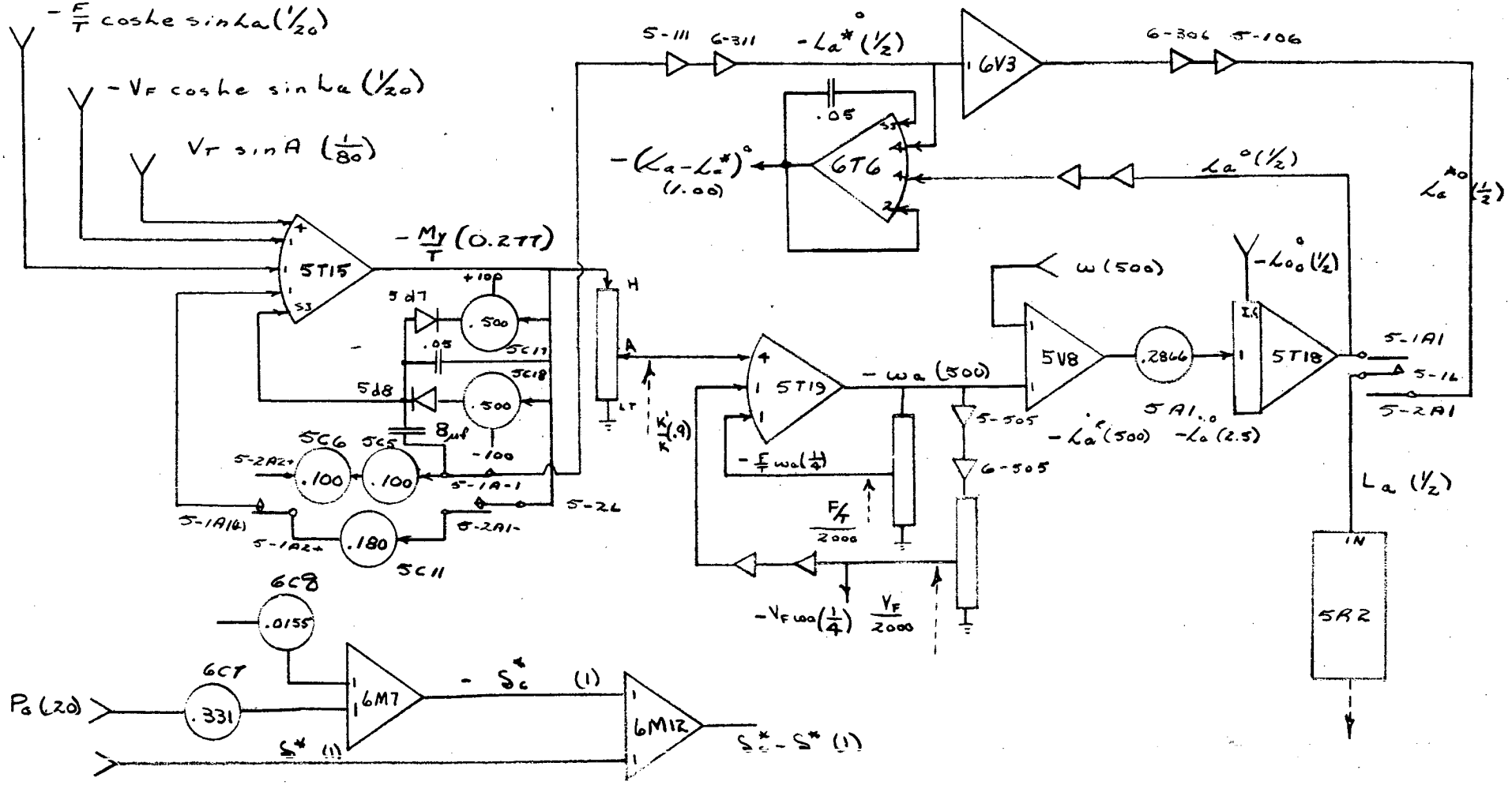

Figure 30 - My/T and La Circuits

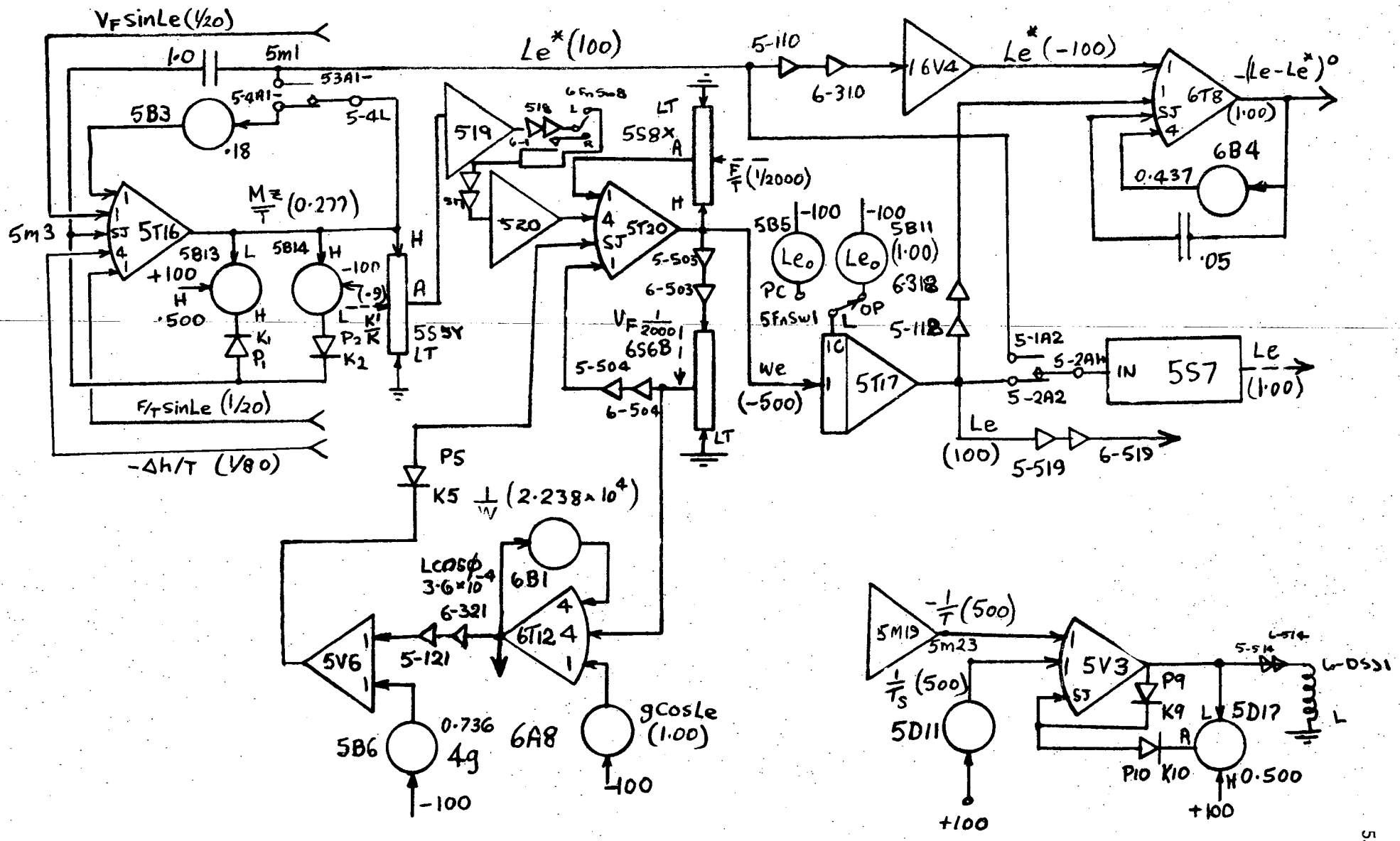

Figure 31 - M_z/T and L_e Circuits

Figure 32 - Atmosphere

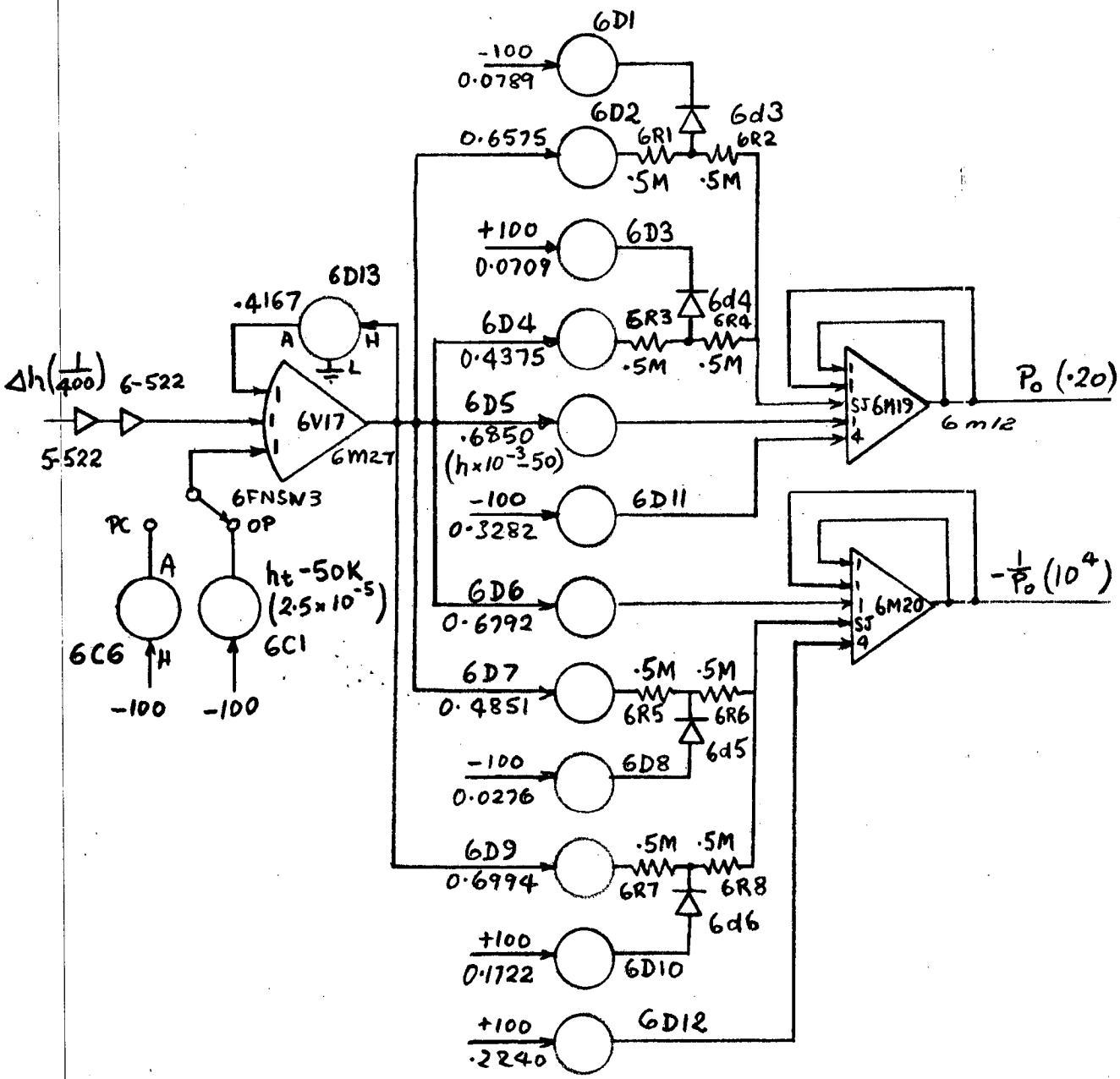

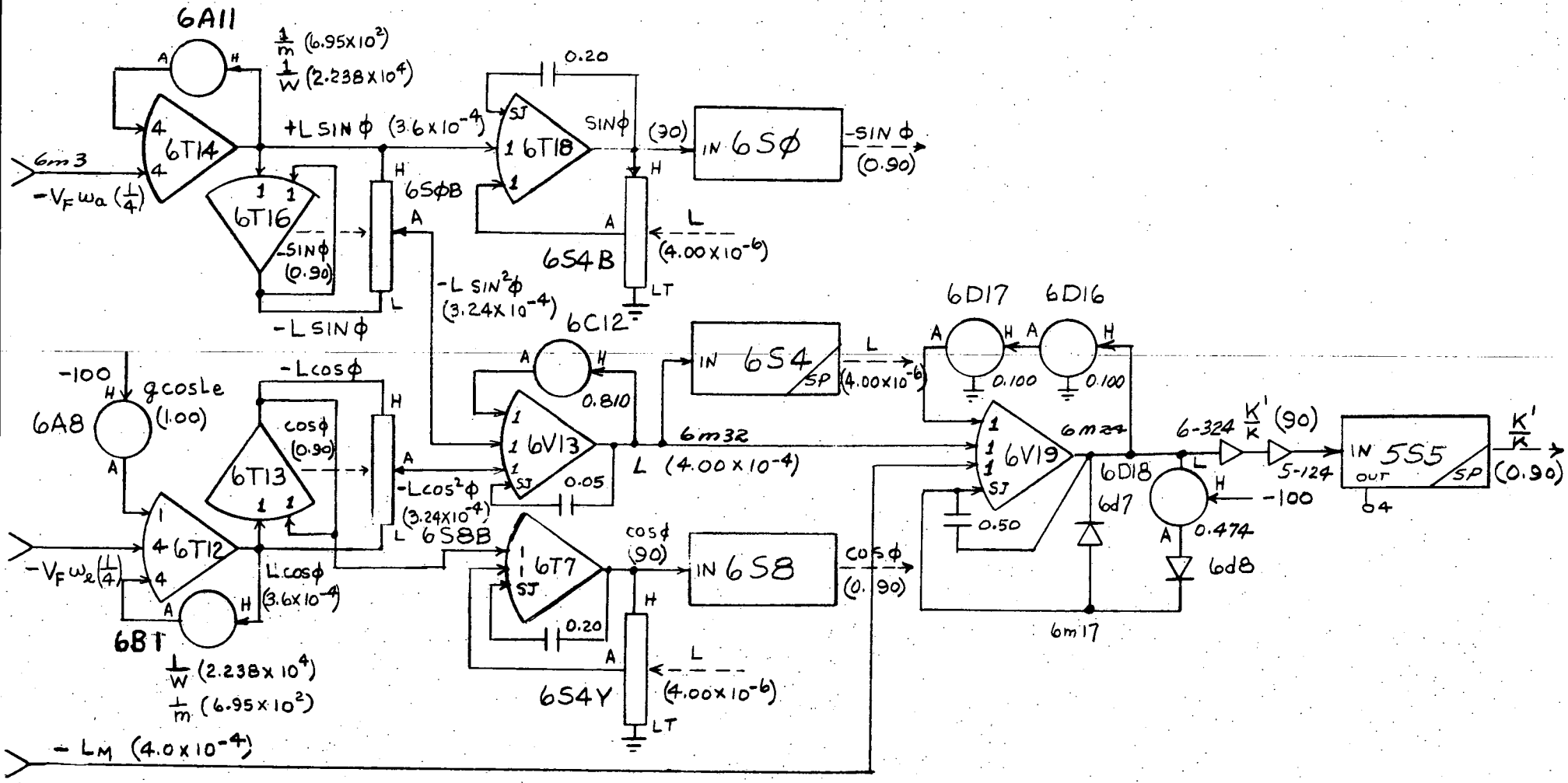

Figure 33 - Bank Angle and Lift Circuit

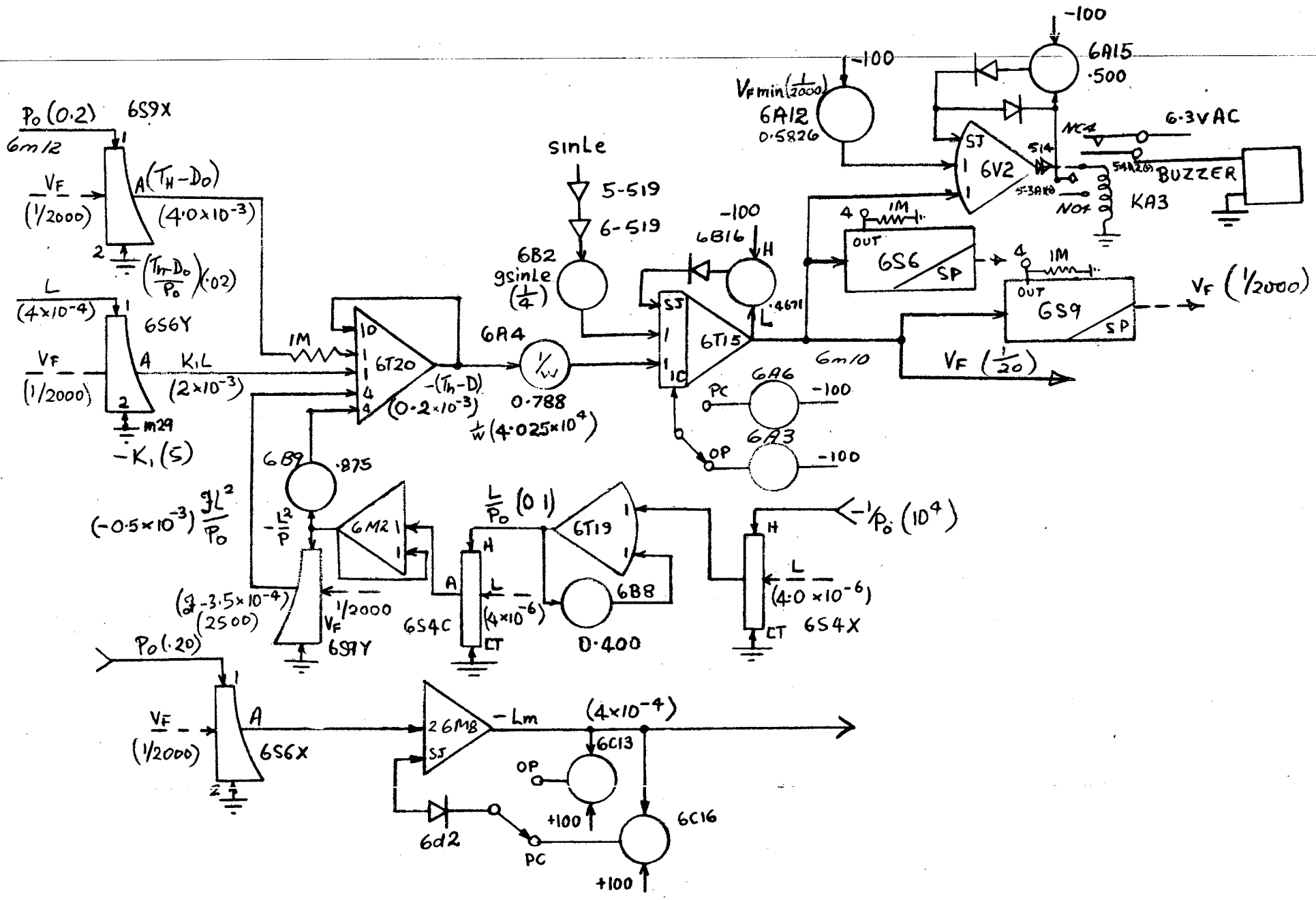

Figure 34 - Velocity and Lift Circuits

Figure 35 - Axis Transformations (1)

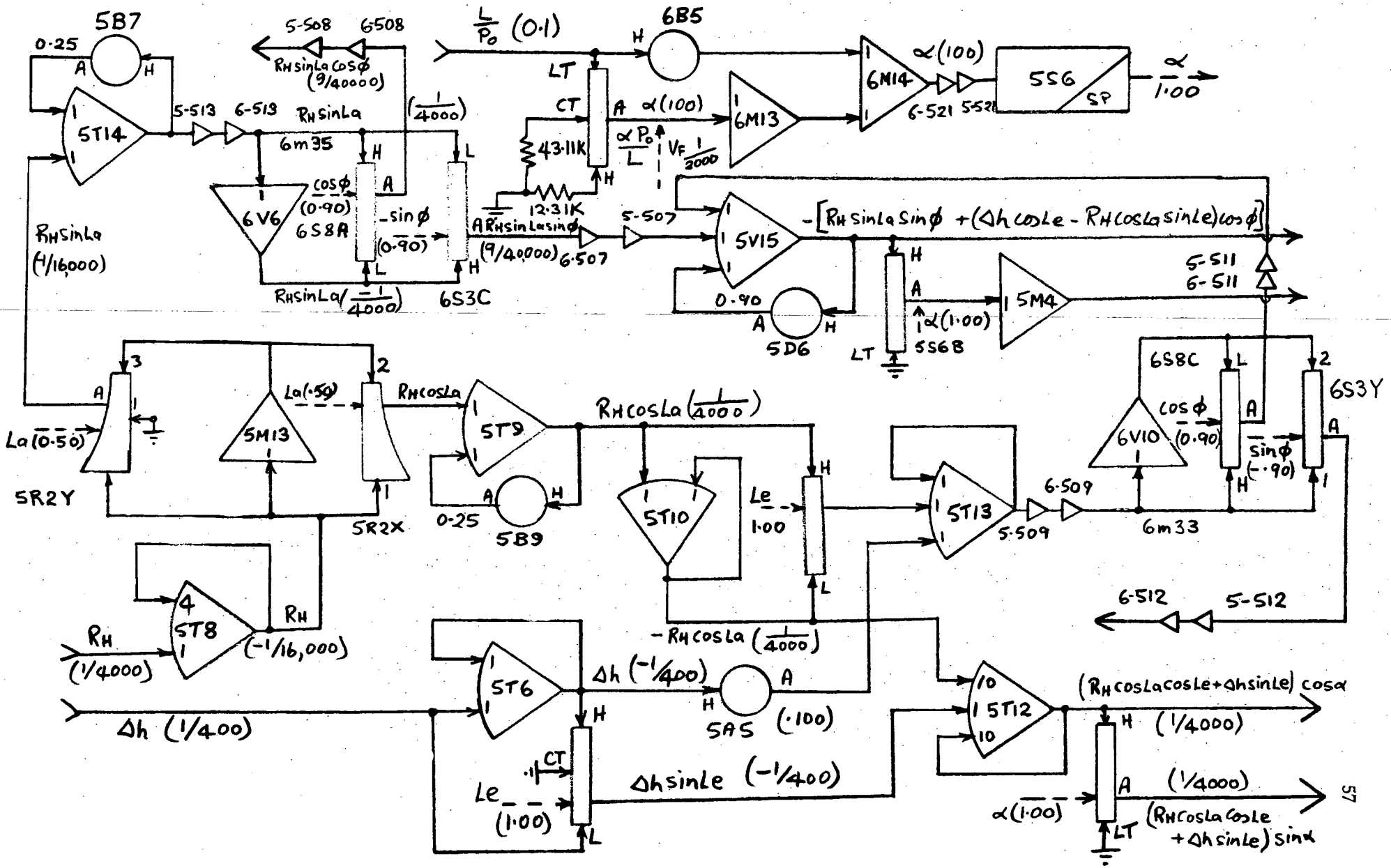

Figure 36 - Axis Transformations (2) and Missile Blinding Circuits

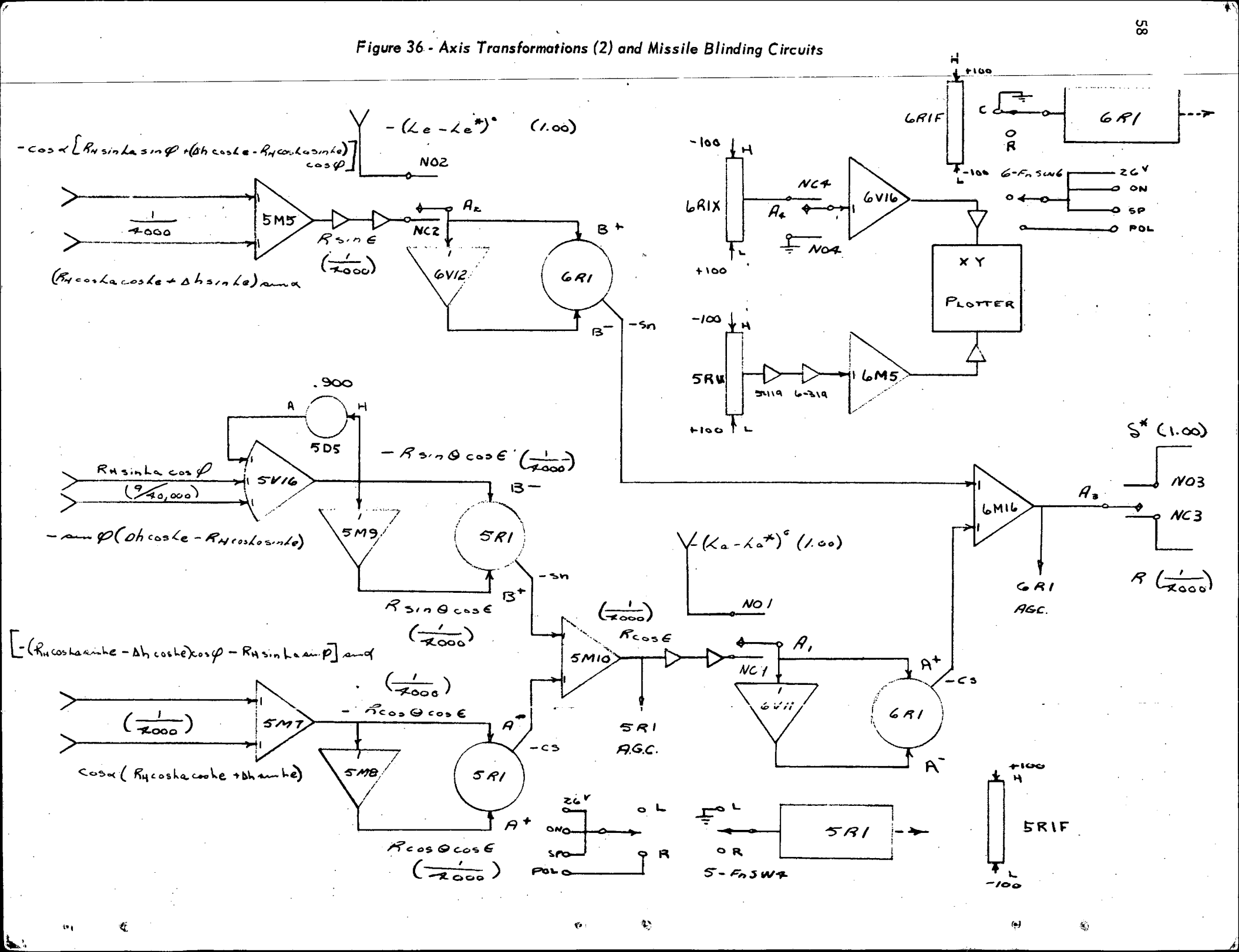

Figure 37 - Automatic Hold and Plotting Board

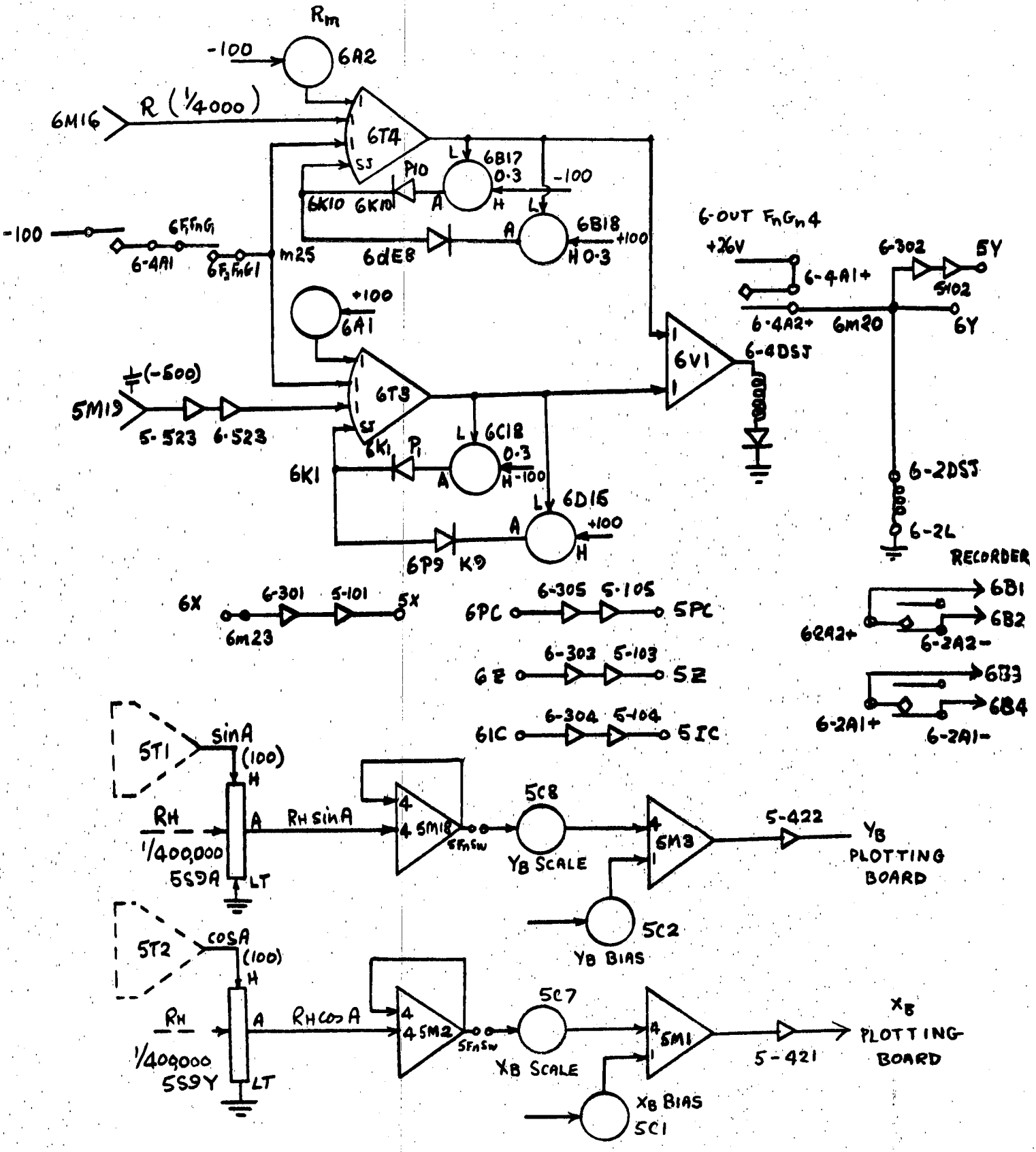

6517005-01

Figure 38 - Remote Control, δ* Relays

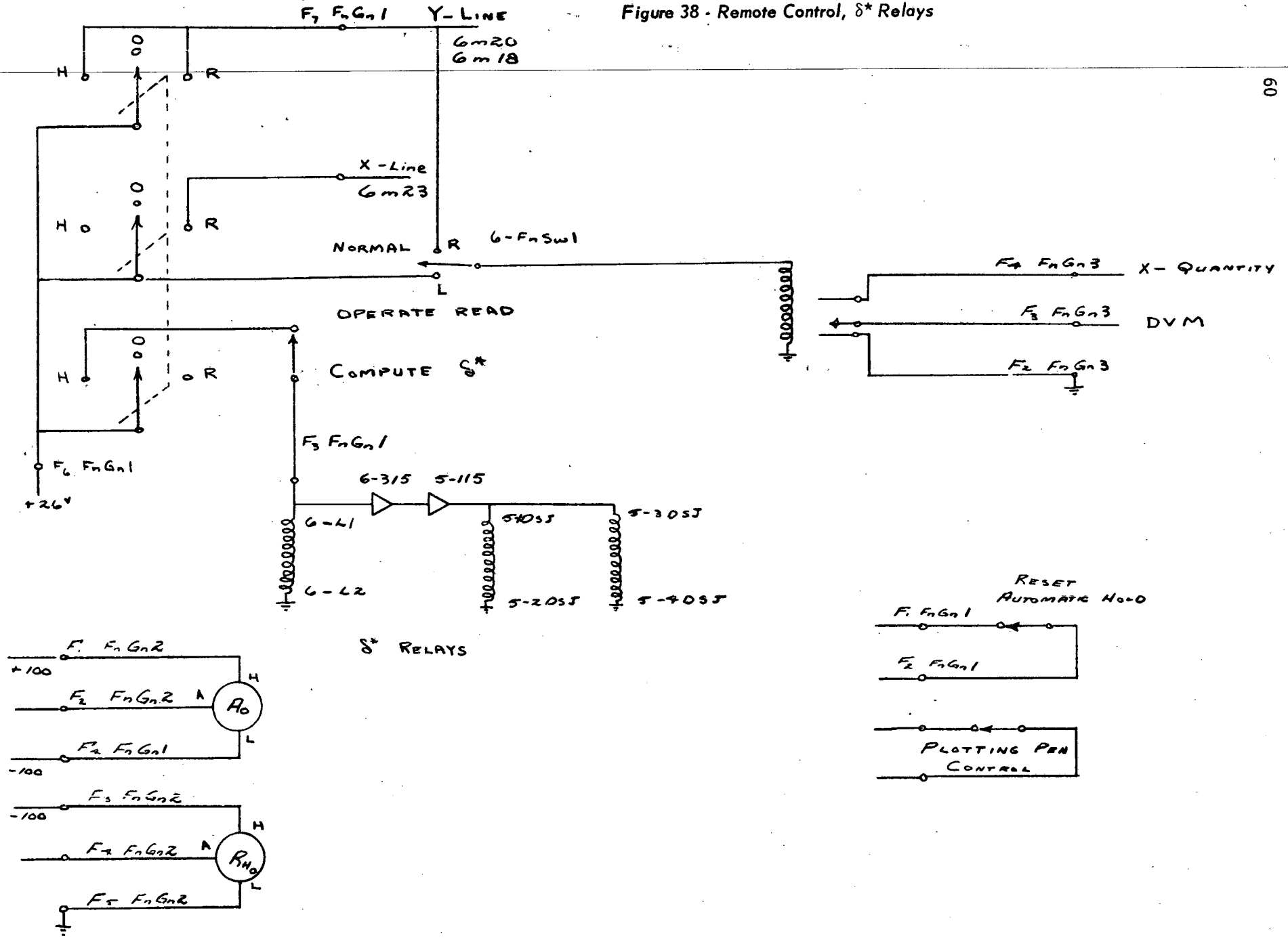

Figure 39 : Time-to-Go for Initiation of Snap-Up

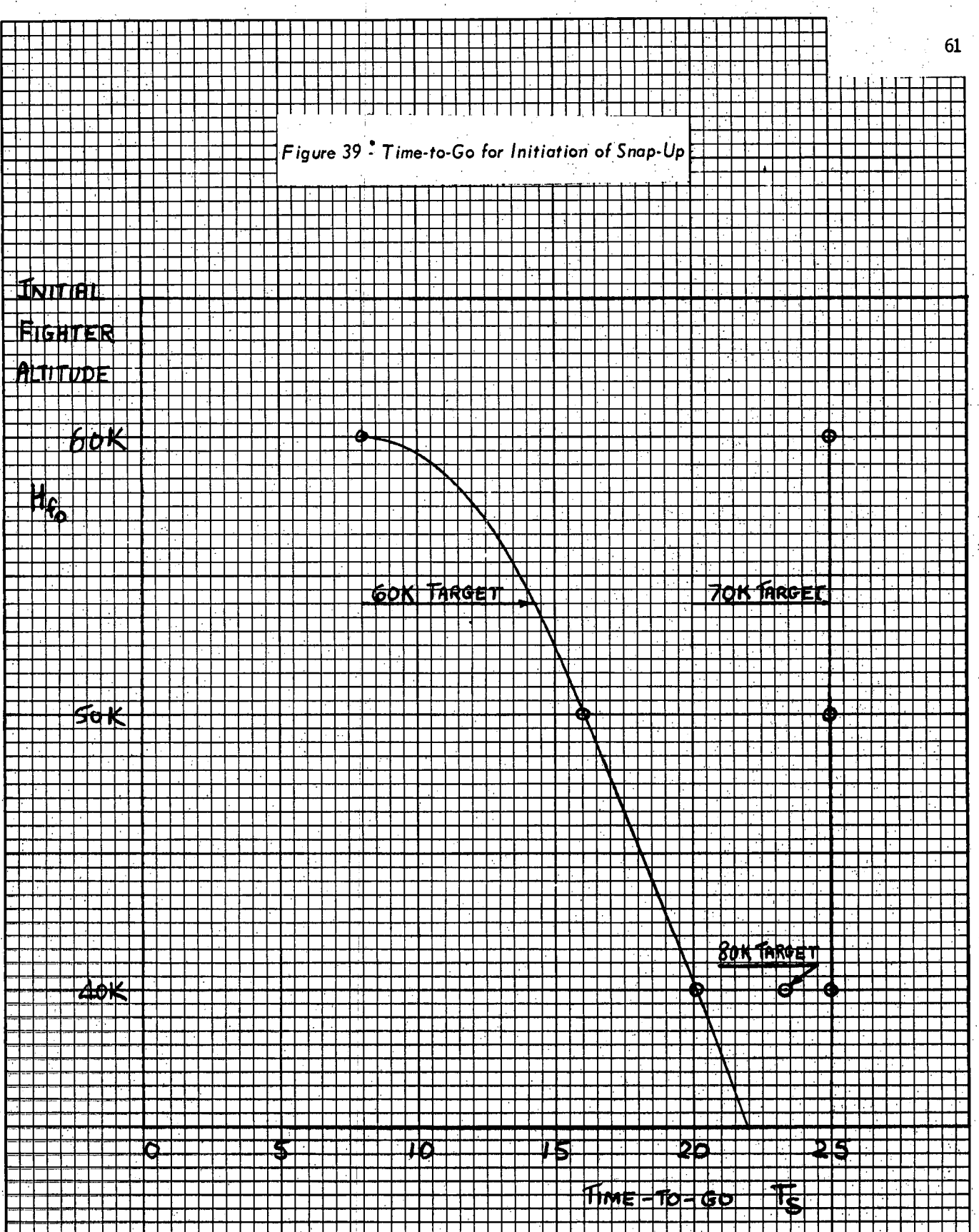

T_S IS INDEPENDENT OF ASPECT AND TARGET SPEED

DEPENDS ON H_{f_0} AND H_T.

ONLY ONE CASE WAS STUDIED FOR 80K TARGET,
IN THE OTHER CASES THE EXACT VALUE OF T_S IS NOT CRITICAL.